New Phytologist

Research

Climate adaptation in *Populus trichocarpa*: key adaptive loci identified for stomata and leaf traits

Marie C. Klein[1], Zi Meng[1], Jack Bailey-Bale[1], Suzanne Milner[1], Peicai Shi[1], Wellington Muchero[2†], Jin-Gui Chen[2], Timothy J. Tschaplinski[2], Daniel Jacobson[2], John Lagergren[2], Matthew Lane[3], Chris O'Brien[3], Hari Chhetri[2], Chanaka Roshan Abeyratne[2], Mengjun Shu[2], Peter Freer-Smith[1], Thomas N. Buckley[1], Troy S. Magney[1], J. Grey Monroe[1], Gerald A. Tuskan[2] and Gail Taylor[1,4]

[1]Department of Plant Sciences, University of California Davis, Davis, CA 95616, USA; [2]Biosciences Division and the Center for Bioenergy Innovation, Oak Ridge National Laboratory, Oak Ridge, TN 37831, USA; [3]Bredesen Center for Interdisciplinary Research and Graduate Education, University of Tennessee Knoxville, Knoxville, TN 37996, USA; [4]Department of Genetics, Environment and Evolution, UCL, London, WC1E6BT, London

Author for correspondence:
Gail Taylor
Email: gail.taylor@ucl.ac.uk

Received: *14 August 2024*
Accepted: *30 March 2025*

New Phytologist (2025) **247:** 2647–2664
doi: 10.1111/nph.70343

Key words: bioenergy, climate adaptation, drought, leaf, *Populus trichocarpa*, stomata.

Summary

- We investigated adaptive genetic variation in *Populus trichocarpa*, a potential biofuel feedstock crop, to better understand how physiological traits may influence tolerance to water limitation. Our study focused on leaf and stomatal traits, given their roles in plant–water relations and adaptation.
- Using a diversity panel of over 1300 genotypes, we measured 14 leaf and stomatal traits under control (well-watered) and drought (water-limited) conditions. We conducted genome-wide association studies (GWAS), climate association analyses, and transcriptome (RNA-seq) profiling to identify genetic loci associated with phenotypic variation and adaptation.
- Stomatal traits, including size and density, were correlated with the climate of origin, with genotypes from more arid regions tending to have smaller but denser stomata. GWAS identified multiple loci associated with trait variation, including a major-effect region on chromosome 10 linked to stomatal size and abaxial contact angle. This locus overlapped with a tandem array of 3-ketoacyl-CoA synthase (KCS) genes and showed strong allele–climate and gene expression associations.
- Our findings reveal genetic and phenotypic variation consistent with local adaptation and suggest that future climates may favor alleles associated with smaller stomata, particularly under increasing aridity. This work provides insights into climate adaptation and breeding strategies for resilience in perennial crops.

Introduction

Altered rainfall patterns and rising temperatures are intensifying drought depth and occurrence, jeopardizing agricultural output (Dai, 2012; Cook *et al.*, 2018; Food and Agriculture Organization of the United Nations *et al.*, 2018). Moreover, in anticipation of the emerging circular bioeconomy, there is a growing need for fast-growing nonfood trees and grasses (Somerville *et al.*, 2010; Clifton-Brown *et al.*, 2019) that can both grow on marginal lands (Schmidt *et al.*, 2015; Mehmood *et al.*, 2017; Hoegh-Guldberg *et al.*, 2018) and tolerate drought and limited nutrient inputs. Consequently, a pivotal challenge is to achieve economically viable yields on marginal lands, in the face of limited water availability (Hoegh-Guldberg *et al.*, 2018; Taylor *et al.*, 2019). Given these challenges, it is crucial to study the physiology and genetics of climate adaptation in potential biofuel crops like poplar (*Populus* spp). Understanding the genetic basis and adaptive value of ecophysiological traits can facilitate the development of varieties that are resilient to arid climates (Stapley *et al.*, 2010; Savolainen *et al.*, 2013; Blumstein *et al.*, 2020).

Collections of diverse genotypes of natural populations in common gardens, originating from wide-ranging environments, are invaluable resources to address these challenges (Taylor *et al.*, 2024). Such collections enable the identification of links between traits and their climates of origin, shedding light on the adaptive value of phenotypic diversity. This can inform predictions of which traits are suitable for dry climates and guide the selection of genotypes for cultivation in arid regions. Additionally, the genetic basis of these traits can be elucidated through this genomic diversity. This exploration is essential for pinpointing genetic markers that can be used to accelerate breeding programs and conservation efforts.

Stomatal traits are central to plant water management and exhibit natural variation in size and density, which have been linked to the climate of origin (Beerling & Woodward, 2008;

Present address: Gail Taylor, Department of Genetics, Evolution and Environment, UCL, London, WC1E 6BT, UK.
†Deceased.

Franks & Beerling, 2009). Smaller and denser stomata, for instance, have often been observed in genotypes from drier climates, suggesting an evolutionary adaptation to aid water conservation and improve plant water-use efficiency (WUE) (McKown *et al.*, 2014a,b, 2019). This association underscores the importance of stomata in local adaptation (Ohsumi *et al.*, 2007; Franks *et al.*, 2009; Doheny-Adams *et al.*, 2012; Sun *et al.*, 2014; Dittberner *et al.*, 2018; Kardiman & Ræbild, 2018). However, the scope of leaf traits influencing water dynamics extends beyond stomata (McKown *et al.*, 2014c). Leaf area, leaf mass, specific leaf area (SLA), photosynthetic potential, surface wettability, and integrated rather than instantaneous WUE form an intricate network that characterizes plant interactions with the environment. Each trait contributes to a plant's ability to conserve water, optimize photosynthesis, and survive in varying conditions of water availability (Benavides *et al.*, 2021). Trade-offs between traits that impact water loss and carbon gain are well known; for example, smaller leaves with higher SLA may transpire less water, and larger leaves might capture more light, balancing the trade-offs between water conservation and energy acquisition (Franks & Beerling, 2009; Hetherington & Woodward, 2003; Liu *et al.*, 2020; Wright *et al.*, 2004, 2017; Wu *et al.*, 2016). Similarly, wettability – the degree of water adhesion to the leaf surface, shaped by cuticle properties and microstructure – plays a key role in regulating leaf temperature and transpiration, aiding water conservation in arid environments (Cavallaro *et al.*, 2022). Structural traits, such as trichome coverage and cuticular wax composition, further influence wettability, affecting stomatal function and photosynthetic efficiency (Aparecido *et al.*, 2017), including cuticular wax composition, which serves as a protective barrier against abiotic stresses (Shepherd & Wynne Griffiths, 2006). It can play an adaptive role in drought response through phenotypic plasticity rather than genetic differentiation (Simões *et al.*, 2020).

At the same time, the direct correlation between total plant water use and yield is also well-established, including for poplar, with high-yielding 'water spending' and lower-yielding 'water saving' strategies varying in their usefulness depending on the intensity, longevity, and life stage of the drought (Tardieu, 2022). Unraveling these conflicting ecological strategies remains challenging.

Although *Populus* trees, as riparian plants, are typically considered vulnerable to drought, notable differences in drought response have been documented among *Populus* genotypes (Tschaplinski *et al.*, 1994, 2006; Marron *et al.*, 2002; Monclus *et al.*, 2006; Street *et al.*, 2006; Huang *et al.*, 2009; Regier *et al.*, 2009; Cocozza *et al.*, 2010; Viger *et al.*, 2013) and the genus can be found across contrasting climate zones, including in extremely arid environments (Brosché *et al.*, 2005). Recognized for its fast growth and high cellulose content, *Populus trichocarpa* stands out as a promising bioenergy crop, including for liquid biofuel production alongside Bioenergy with Carbon Capture and Storage (BECCS). In addition, *Populus* is a valuable model for genetics and plant biology research (Tuskan *et al.*, 2006; Kačík *et al.*, 2012; Taylor *et al.*, 2019), and extensive research has provided substantial evidence of local adaptation to the climatic conditions of its native habitats (McKown *et al.*, 2014a,b,c; Evans *et al.*, 2014, 2016; Porth & El-Kassaby, 2015; Zhang *et al.*, 2019; Blumstein *et al.*, 2020; Apuli *et al.*, 2021). Such attributes augment the significance of *P. trichocarpa* trees in achieving the U.S. Department of Energy's ambitious Sustainable Aviation Fuel (SAF) target by 2050, while simultaneously reducing life cycle greenhouse gas emissions by at least 50% (U.S. Department of Energy, 2022; U.S. Department of Energy et al., 2022).

To assess the degree of local adaptation of leaf and stomatal traits, we established a common garden of black cottonwood (*Populus trichocarpa*) in Davis, California, an extremely hot and dry site. These trees are derived from a natural population from the Pacific Northwest, representing a wide spectrum of climates (Gornall & Guy, 2007; Evans *et al.*, 2014; McKown *et al.*, 2014a). In this study, we investigated the role and importance of 14 leaf physiology traits related to leaf morphology, stomata, and water use in *P. trichocarpa* under both drought and well-watered conditions. We conducted field campaigns to measure leaf and stomatal traits twice during the summer growing season in a subsample of *c.* 469 unique genotypes (Fig. 1, Supporting Information Fig. S1d,e; Table S1). We measured biomass yield traits in the whole population (*c.* 1382 unique genotypes). In doing so, we explored the adaptive signature of drought tolerance and plastic responses in this widely divergent population. To overcome the difficulties associated with phenotyping a large number of samples, we employed a suite of automated phenotyping algorithms for data acquisition. Among leaf traits, we also assessed $\delta^{13}C$ of *c.* 469 unique genotypes–a metric for WUE in wood sampled during tree dormancy, shown in *Populus* to be valuable and correlated with WUE (Viger *et al.*, 2016; Bogeat-Triboulot *et al.*, 2019). The goal of our study was to explore the relationship between trait variation and climate of origin, assessing the adaptive value of trait variation, their relevance and usefulness to trait selection for drought tolerance, and the roles of plastic acclimatory responses. Finally, genome-wide association analyses (GWAS) were conducted to characterize the genetic basis of these traits, enabling a more holistic view of climate–genotype–trait relationships in *P. trichocarpa* that reflects local adaptation and provides gene targets for future tree improvement for the emerging bioeconomy.

Materials and Methods

Field site and plant material

The research was conducted on a 6.1-ha plot at the UC Davis Plant Science Field Facility in Davis, CA (38°32′47.4″N, 121°47′32.7″W) (Fig. 1a), as described previously (Taylor *et al.*, 2024). The experimental layout of the whole site consisted of drought and control treatments across adjacent fields divided into three distinct blocks arranged in an incomplete randomized block design. The *Populus trichocarpa Torr.* & *Gray* population used in this study was sourced from a range of latitudes exhibiting diverse climate and rainfall patterns, representative of most of the species' habitats (38.9–54.3°N, 116–128.7°W), and included a total of 1382 genotypes (Fig. 1a). *P. trichocarpa* cuttings were received and planted in a glasshouse on February 1, 2020. On

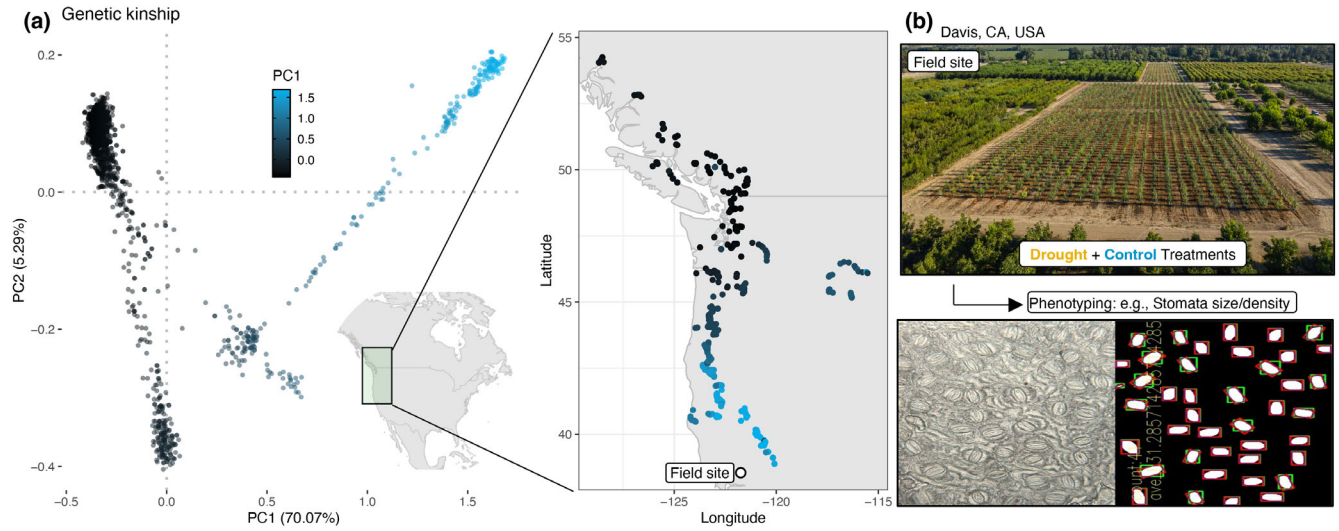

Fig. 1 Overview of population structure of *Populus trichocarpa* and experiment in Davis, CA. (a) Principal components of genetic kinship among *P. trichocarpa* genotypes and their locations of origins in the Pacific Northwest. (b) Common garden located below and an example of stomatal phenotyping. On the left: raw microscopy image; on the right: processed image suitable for identifying stomatal density and size, captured at 16× magnification.

March 30, 2020, they were relocated to a lath house to harden. Subsequently, 7628 trees were transplanted to the field on April 10, 2020, with 782 unique genotypes in the drought field site and 1382 unique genotypes in the control field site, reflecting the availability of viable cuttings. A single row of *P. trichocarpa* border trees (not used for measurements) was established around the experimental trees in each replicate block to reduce the effect of undesired edge effects.

Drought treatment

We employed surface drip irrigation, applying a set water volume measured with flow meter sensors, OMNI™ + Turbo (T^2) Water Meters, at each treatment site throughout the field season. Trees were fully irrigated until March 2021 to conclude their first establishment year. Following this, the irrigation was reduced in the drought treatment to achieve a soil moisture deficit of 150 centibars (0.15 MPa) from March to December 2021. This deficit was significant in comparison with the fully irrigated (control) treatment, representing a long-term modest drought throughout the growing season. During the 2021 field season, soil moisture was monitored using Watermarks (Granular Matrix Sensors from MMM) (for daily soil water potential) and neutron probes (for volumetric water content every 12 d) across seven stations, with distinct placements for varying irrigation conditions. The comprehensive data, covering topsoil to a depth of 120 cm, verified *c.* 50% reduction in soil moisture for the drought treatment compared to the control, aiding our evaluation of drought's impact on plant performance and WUE (Fig. S1). Soil moisture levels were systematically assessed during the 2021/2022 and 2022/2023 field seasons by using two primary techniques: (1) soil water potential was regularly recorded using Watermarks, equipped with remote daily data logging; and (2) volumetric water content was determined using a neutron probe at 12-d intervals (Taylor *et al.*, 2024) (Fig. S1).

The data collected from these sensors, encompassing both topsoil and deeper soil layers, were crucial in monitoring. The significant difference in soil moisture levels was used to assess the impact of drought on crop performance and WUE (Fig. S1).

Core population and sampling

We defined a subsample of unique genotypes that were fully replicated in a randomized complete block design in triplicate in both drought and control treatments, and this population is referred to as the 'core population, $n = 469$ genotypes'.

For leaf phenotyping, encompassing stomatal traits and leaf area measurements (Table S1), we conducted comprehensive sampling of the core population at two specific time points: June (1 month after the drought treatment initiation) and September (106 d after the first collection, which includes an extended period of drought). However, note that some trees were lost due to mortality in the field (Table S2), and not all phenotyping was completed in all blocks (Fig. S1d,e).

In June, we sampled all of the core population of the drought treatment (Drought blocks 1, 2, and 3; $n = c.\ 3 \times 469$), and in the core population control treatment, we sampled only block 2 ($n = 469$). Similarly, in September, we sampled the core population in blocks 1, 2, and 3 ($n = 3 \times 469$) of the drought and only block 2 ($n = 469$) in the control, given time constraints for sampling and analysis. In summary, our analysis encompassed a total of 1861 trees from both the June and September samplings, comprising 422 unique genotypes (441 trees) from the control group and 468 unique genotypes (1420 trees) from the drought treatment. For further clarity, please refer to Fig. S1(c,d). Wood sampling for carbon isotope discrimination (Table S1) was performed on the whole 'Core' population of all 6 blocks (469 genotypes, $n = 3019$ samples including replicates) in January 2022.

Climatic data

Climatic data were sourced from WorldClim fit to western North America, which contains a set of global climate layers with high spatial resolution (2.5′), averaging across the years 1970–2000 (Fick & Hijman, 2017). The WorldClim database provides interpolated climate data (a total of 19 variables), including temperature, precipitation, and derived bioclimatic variables, facilitating a comprehensive understanding of the environmental climates of origins for our population of *P. trichocarpa* trees.

Climate variables are the following:

Bio 1 Annual Mean Temperature.

Bio 2 Mean Diurnal Range (Mean of monthly (max temp – min temp)).

Bio 3 Isothermality.

Bio 4 Temperature Seasonality (SD × 100).

Bio 5 Max Temperature of Warmest Month.

Bio 6 Min Temperature of Coldest Month.

Bio 7 Temperature Annual Range.

Bio 8 Mean Temperature of Wettest Quarter.

Bio 9 Mean Temperature of Driest Quarter.

Bio 10 Mean Temperature of Warmest Quarter.

Bio 11 Mean Temperature of Coldest Quarter.

Bio 12 Annual Precipitation.

Bio 13 Precipitation of Wettest Month.

Bio 14 Precipitation of Driest Month.

Bio 15 Precipitation Seasonality (Coefficient of Variation).

Bio 16 Precipitation of Wettest Quarter.

Bio 17 Precipitation of Driest Quarter.

Bio 18 Precipitation of Warmest Quarter.

Bio 19 Precipitation of Coldest Quarter.

Genotypic data

The reference genome and resequencing of the *Populus trichocarpa* population (1523 genotypes) were conducted by the U.S. Department of Energy Joint Genome Institute (Tuskan *et al.*, 2006; Evans *et al.*, 2014) and are accessible via the Joint Genome Institute Database. We used Genome version: *Populus trichocarpa* v.4.1, Phytozome genome ID: 533. Genotypic data were derived from high-coverage whole-genome resequencing. Short reads were aligned to the *P. trichocarpa* reference genome (v.3.0) using BWA, with mate pair metadata corrected and duplicate molecules marked using Picard tools. Variants, including single nucleotide polymorphisms (SNPs) and small indels, were called using SAMtools and bcftools (Evans *et al.*, 2014).

Leaf sampling

Two fully expanded, first and second-mature leaves, specifically the fifth leaf from the apex on each of two south-facing primary branches, were collected at a height of *c.* 1.3 m and lightly misted with water, sealed in plastic bags, and stored in a cooler box on ice. These samples were immediately returned to the laboratory and subsequently kept at 4°C in a refrigerated room. All phenotypic analyses were initiated within 48 h of collection.

Stomatal imprinting and imaging For the assessment of stomatal morphology, imprints were collected from the right abaxial portion of the leaf section and sampled as previously described (Tricker *et al.*, 2004). A designated rectangular patch of this surface received a coating of clear nail polish. Upon drying, a strip of clear adhesive tape was utilized to lift off a thin layer, capturing a majority of epidermal cells and stomata. The tape was then placed on a microscopic slide and stored until further processing. This methodology resulted in a comprehensive collection of 1869 imprints of all leaves collected (e.g. in Fig. 1b). The imaging phase involved using two Zeiss Standard 16× microscopes, each equipped with camera attachments. All imaging procedures used TCapture software (v.5.1.1).

Stomatal detection and analysis To identify stomatal cells in our imprints, we integrated a model rooted in the U-Net architecture conceived within the PyTorch framework. The image data underwent a preliminary preprocessing stage and was transitioned into tensor format. Using a dataset of 300 representative images for training, our model was meticulously calibrated to distinguish stomatal cells in the imprints efficiently. During the predictive phase, the OpenCV, imported as cv2 (https://pypi.org/project/opencv-python/) software library, facilitated the demarcation of the tightest bounding rectangle around every detected stomatal cell, an integral step for gauging its geometric characteristics. Our analytical process resulted in the calculation of the average stomatal dimensions for each individual imprint (e.g. in Fig. 1b).

Leaf area and perimeter One of the two sampled leaves was used to measure leaf area (LA) and perimeter (PI). We used a Canon EOS Rebel T7i camera positioned over a lightbox (AGPTEK – Model A3USB) to photograph the leaves alongside a scale bar next to the leaves. Subsequently, these images were analyzed further at Oak Ridge National Laboratory (Oak Ridge, TN, USA). In this process, iterative thresholding was applied to the gray-scaled image to separate the lightbox from the rest of the image, from which the leaf segmentation was extracted and rotated to achieve axis symmetry before being cropped to the leaf's bounding box. Once the leaf was distinguished from the petiole, various leaf features, including LA and PI, were reliably detected and recorded. The analysis was completed using the SCIPY (v.1.11.4) and SCIKIT-IMAGE (v.0.19.3) libraries in PYTHON.

Dry weight and fresh weight We measured the fresh weight of one of the two selected leaves, the same leaf that was photographed for the leaf perimeter, area, and fresh weight, using a precision balance (Adam Equipment – PGW 453e). Following this, the leaf was dried for 48 h in a paper bag at 80°C and re-weighed for dry weight. To prevent moisture absorption, all dried leaves were stored with silica desiccant beads.

Contact angle (wettability) Leaf contact angles were measured as described by Kwon *et al.* (2014). A water droplet was placed on the left side of the leaf, while the right side was used for stomatal traits. To initiate the process, we prepared two leaf disks, which were subsequently taped to a microscope slide. For each leaf disk, a distilled water droplet was applied by a pipette. Subsequently, we captured images of the contact surface using a Canon EOS 500D camera. Similar to stomatal detection, we used a convolutional neural network implemented in PyTorch to distinguish water droplets following the region-growing methodology (Lagergren *et al.*, 2023). Using a dataset of 96 images for training and 23 for testing, we achieved a segmentation accuracy (Sørensen-Dice coefficient) of 0.917. Contact angle was measured by fitting a circle to the detected droplets using a Hough transform (Xu *et al.*, 2013), and subsequently measuring the angle of the droplet to the microscope slide.

Spectral reflectance Spectral reflectance was measured on the adaxial surface of each leaf utilizing a handheld PolyPen RP 410 (Photon Systems Instruments) after samples were returned to the field. The data were subsequently captured and recorded using the SpectraPen software provided by the manufacturer. We used a Spectralon white reference standard to normalize reflectance measurements. From the reflectance spectra, we computed NDVI, defined as the Normalized Difference Vegetation Index (see calculations in Table S1), and PRI, defined as the Photochemical Reflectance Index (see calculations in Table S1).

Wood sampling

Preparation for $\delta^{13}C$ Wood samples for $\delta^{13}C$ analysis were collected in January 2022 from the Core population across all three blocks of both treatments (control and drought), totaling 3019 samples from 479 genotypes. For each sample, three 5-cm segments were harvested from south-facing primary branches at *c.* 1.3 m height and stored in labeled paper bags. The samples were dried at 65°C for 14 d to ensure consistent moisture removal.

Following drying, dormant buds at branch tips were carefully removed using shears, while the bark was left intact. The dried wood was ground to a fine powder using a TissueLyser II (Qiagen) with stainless steel grinding jars (2 × 10 ml) at 20 Hz for 1 min, yielding a particle size of *c.* 0.50 grains mg^{-1}, following a protocol similar to Moghaddam *et al.* (2013). Ground samples were transferred into labeled plastic vials, and precisely 3 mg (±10%) of powder was measured into tin capsules, which were folded as necessary for analysis. The capsules were arranged in 96-well plates, with two duplicates included in each of the 33 plates.

The prepared samples were sent to the UC Davis Stable Isotope Facility for carbon isotope discrimination analysis using isotope-ratio mass spectrometry (IRMS).

Calculations of $\delta^{13}C$ The following was used to calculate $\delta^{13}C$:

$$\delta^{13}C = \left(\left({}^{13}C/{}^{12}C\right)\text{standard}\right)/\left(\left({}^{13}C/{}^{12}C\right)\text{sample}\right) \times 1000‰$$

This value is expressed in parts per thousand (‰) and compares the ratio of ^{13}C to ^{12}C in the sample to that in a standard (typically a belemnite formation from the Peedee Formation in South Carolina, known as PDB). A negative $\delta^{13}C$ value implies that the $^{13}C/^{12}C$ ratio in the plant is lower than that in the standard. Since plants discriminate against $\delta^{13}C$, most plants have negative $\delta^{13}C$ values. The more negative the value, the stronger the preference for ^{12}C in the photosynthetic process. A higher WUE is indicated by a higher $^{13}C/^{12}C$ ratio (less negative $\delta^{13}C$ values and less discrimination against ^{13}C).

Tree height

Biomass productivity data were collected as tree height measurements in March 2021 (beginning of the growing season, after leaf flush) and November 2021 (end of growing season, after bud set), following the first year of the applied drought treatment. The height of every experimental tree across each block of both treatments was recorded using a telescopic height pole.

Statistical analysis

Statistical analyses were performed using RSTUDIO (v.4.1.2). We visualized spatial data using the LEAFLET package (v.1.7.1), a JavaScript library for interactive maps. After loading the necessary library, our geospatial data were overlaid on a CartoDB Positron basemap on which the data points can be placed. During the data exploration and organization phases, we employed a suite of packages including DPLYR, TIDYVERSE, TIDYR, PLOTRIX, DATA.TABLE, and STRINGR. Enhanced data visualization was achieved with the GGPLOT2 package, facilitating the creation of frequency diagrams, reaction norms, and boxplots. For statistical significance testing and analysis of variance (ANOVA), we utilized packages such as STATS, LME4, EMMEANS, and LMERTEST.

Water content The water content (WC) was calculated using the fresh weight and dry weight of leaf samples. The WC was also calculated by using (see Table S1):

$$WC = (\text{fresh weight (g)} - \text{dry weight (g)})$$

Proportional water content (PWC) was also calculated by using (see Table S1):

$$PWC = (\text{fresh weight (g)} - \text{dry weight (g)})/\text{fresh weight (g)}$$

Drought response To quantify the plasticity of the trait, we employed the formula:

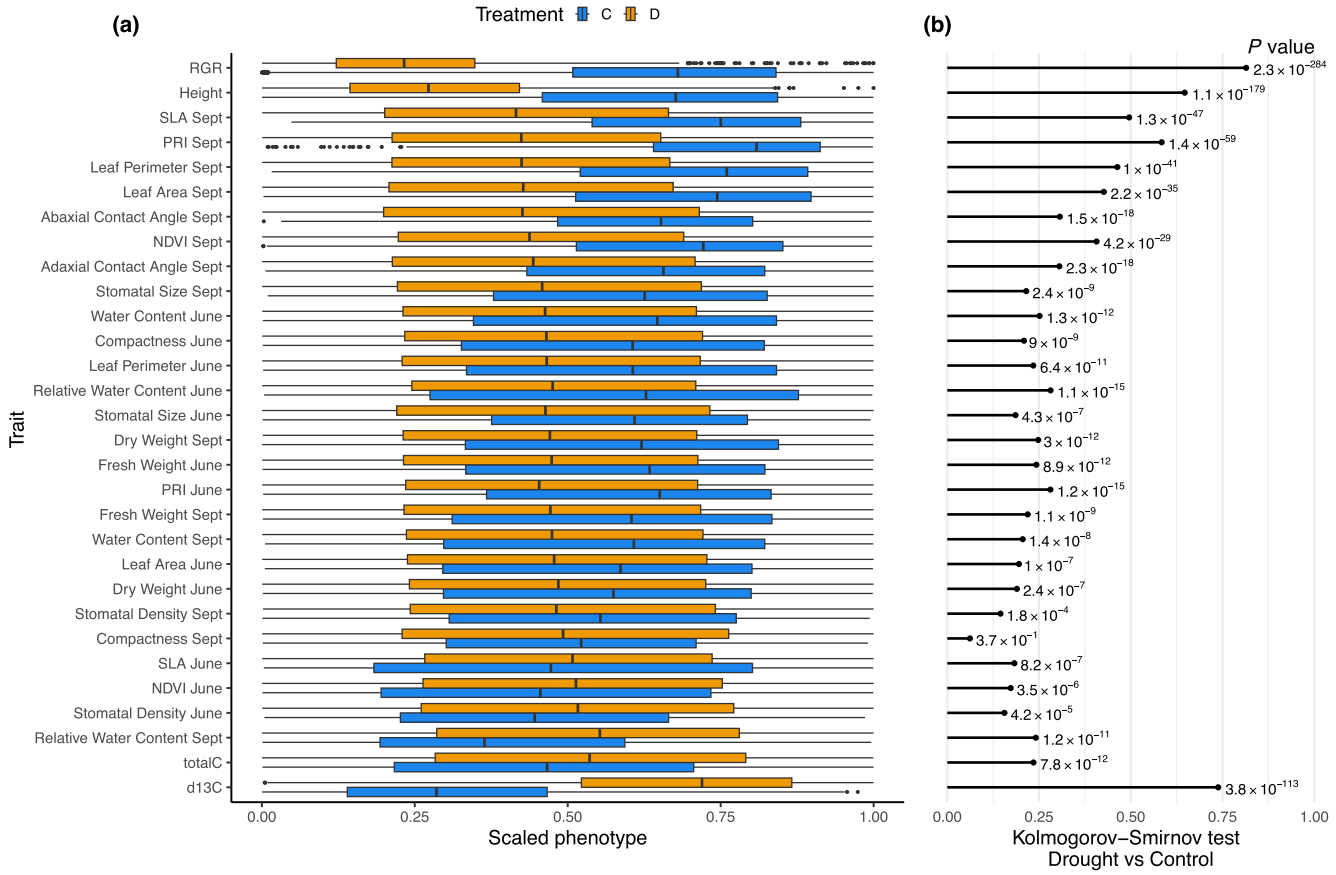

Fig. 2 Phenotypic responses to drought and control treatments in *Populus trichocarpa*. (a) Inverse normal transformation (INT) scaled phenotypes for traits under control (C, blue) and drought (D, orange) treatments. (b) Kolmogorov–Smirnov test statistic and corresponding *P*-values comparing trait distributions between treatments.

$$\text{Drought Plasticity Index} = (\text{Mean Trait Value under Control} - \text{Mean Trait Value under Drought})$$

This index provided a relative difference value, representing the extent of trait variation due to drought exposure across different genotypes (Fig. 2; Table S3).

Drought resilience index (DRI)

$$\text{DRI} = (\text{phenoD}/\text{phenoC})/(\text{mean phenoD}/\text{mean phenoC})$$

where phenoD is phenotype drought, phenoC is phenotype control, mean phenoD is population mean of phenotype D, and mean phenoC is population mean of phenotype C.

This index calculates the ratio of yield reduction under stress in a specific genotype relative to the average reduction across all genotypes (Table S4). PhenoD refers to a phenotype of the drought treatment, and phenoC refers to a phenotype of the control treatment.

Relative growth rate The relative growth rate (RGR) of height was calculated with the equation:

$$\text{RGR} = \left(\log_e(W_2) - \log_e(W_1)\right)/\left(\log_e(W_1)\right)$$

where W_1 represents the height taken in March 2021 and W_2 represents the height measured in November 2021.

Estimating correlations and variance components of traits

In our analysis, the contribution of Genotype (G), Treatment (T), and their interaction (G : T) to the variance in plant traits was estimated. This estimation was conducted in R, utilizing the lme4 package, where Genotype, Treatment, and Interaction were treated as random effects. Post-model fitting, the variance components were extracted using the VarCorr function, and the variance associated with Genotype, Treatment, Interaction, and Residual was isolated. The total variance was computed as the sum of these components. Subsequently, the percent variance explained by each component was calculated by dividing each variance component by the total variance and multiplying by 100 (Fig. S2). To estimate the relationships between plant traits, pairwise Pearson correlation coefficients were calculated separately for control and drought treatments in R with cor (. . ., use="complete.obs"). These correlations were visualized with a heatmap in R (Fig. S3).

$$\text{Model}: y_{ijk} = \mu + G_i + T_j + (G \times T)_{ij} + \epsilon_{ijk}$$

where y_{ijk} represents the observed trait value for the i^{th} genotype, j^{th} treatment, and k^{th} observation. μ is the overall mean of the trait across all genotypes and treatments. G_i represents the random effect of the i^{th} genotype. T_j represents the fixed effect of the j^{th} treatment. $(G \times T)_{ij}$ is the random interaction effect between the i^{th} genotype and j^{th} treatment. ε_{ijk} denotes the residual error term associated with each observation, capturing the variability not explained by the other components in the model.

The percent variance explained by each component is calculated as follows:

$$\%\text{Variance Component} = (\text{Variance Component}/\text{Total Variance}) \times 100$$

Estimation of broad-sense heritability H^2 for traits and genetic correlation

An upper limit of broad-sense heritability, which is clonal repeatability, for a total of 30 traits was calculated by estimating genetic variance as per the univariate model below:

$$\boldsymbol{y} = \boldsymbol{1}\mu + \boldsymbol{Z}\boldsymbol{g} + \boldsymbol{e}$$

$$\boldsymbol{g} \sim N\left(0, \sigma_g^2 I\right); \boldsymbol{e} \sim N\left(0, \sigma_e^2 I\right)$$

$$H_R^2 = \left(\sigma_g^2\right) / \left(\left(\sigma_g^2 + \sigma_e^2\right)\right)$$

Here, $\boldsymbol{y}$ is an $(\boldsymbol{n} \times \boldsymbol{1})$ vector of transformed trait values for all ramets (n) for a given trait in either drought or control treatment. The trait mean is denoted by μ, and $\mathbf{1}$ is a $(\boldsymbol{n} \times \boldsymbol{1})$ vector of ones. The vector $\boldsymbol{g}$ is a $(\boldsymbol{i} \times \boldsymbol{1})$ vector of total genetic effects for i individual genets, modeled by the $(\boldsymbol{n} \times \boldsymbol{i})$ incidence matrix $\boldsymbol{Z}$, and σ_g^2 represents the total genetic variance. $\boldsymbol{e}$ is an $(\boldsymbol{n} \times \boldsymbol{1})$ vector of random residuals, and σ_e^2 is its variance estimate.

$\boldsymbol{I}$ represents an identity matrix of corresponding dimensions and ignores the relatedness among genets when modelling $\boldsymbol{g}$. The following bivariate model was used to estimate trait–trait covariance for each pair of traits thus making it possible to calculate pair-wise genetic correlation (r_g).

$$\begin{bmatrix} \boldsymbol{y_{t1}} \\ \boldsymbol{y_{t2}} \end{bmatrix} = \begin{bmatrix} \mathbf{1}_{(n\times 1)} & \mathbf{0}_n \\ \mathbf{0}_n & \mathbf{1}_{(n\times 1)} \end{bmatrix} \begin{bmatrix} \mu_{t1} \\ \mu_{t2} \end{bmatrix} + \begin{bmatrix} \boldsymbol{Z_{t1}} & \mathbf{0}_{(n\times i)} \\ \mathbf{0}_{(n\times i)} & \boldsymbol{Z_{t2}} \end{bmatrix} \begin{bmatrix} \boldsymbol{g_{t1}} \\ \boldsymbol{g_{t2}} \end{bmatrix} + \begin{bmatrix} \boldsymbol{e_{t1}} \\ \boldsymbol{e_{t2}} \end{bmatrix}$$

$$\begin{bmatrix} \boldsymbol{g_{t1}} \\ \boldsymbol{g_{t2}} \end{bmatrix} \sim \mathbf{N}\left(\mathbf{0}_{(2i\times 1)}, \boldsymbol{T^*}\right)$$

$$\boldsymbol{T^*} = \mathbf{T} \otimes \boldsymbol{I}$$

$$\boldsymbol{T} = \begin{bmatrix} \sigma_{t1}^2 & \sigma_{t1t2} \\ \sigma_{t1t2} & \sigma_{t2}^2 \end{bmatrix}$$

$$r_g = \frac{\sigma_{t1t2}}{\sqrt{\sigma_{t1}^2} \times \sqrt{\sigma_{t2}^2}}$$

Here, $\boldsymbol{y_{t1}}$ and $\boldsymbol{y_{t2}}$ are $(\boldsymbol{n} \times \boldsymbol{1})$ vectors with trait values for the pair of traits under consideration (t_1 and t_2), while μ_{t1} and μ_{t2} are means for each trait, respectively. $\boldsymbol{g_{t1}}$ and $\boldsymbol{g_{t2}}$ represent $(\boldsymbol{i} \times \boldsymbol{1})$ vectors of total genetic values for t_1 and t_2 respectively modeled by the $(\boldsymbol{n} \times \boldsymbol{i})$ $\boldsymbol{Z_1}$ and $\boldsymbol{Z_2}$ incidence matrices. Covariance of genetic values was modeled by $\boldsymbol{T}^*$ and was obtained as the Kronecker product ($\otimes$) between $\boldsymbol{I}$ and $\boldsymbol{T}$ matrices. For both univariate and bivariate models described above, solving linear mixed model equations, obtaining REML estimates of variance covariance components, and obtaining SE of statistics were carried out as per the methods described in Lynch & Walsh (1998), and implemented in Covarrubias-Pazaran (2016) (Fig. S4).

Climate–trait correlations For assessing relationships between traits (separately for drought and control treatments) and climate of origin (Bioclimatic variables 1–19 from WorldClim) of experimental trees (Table S5), Spearman's rank correlation coefficient was computed using R (Fig. 3a). The Spearman's correlation measures the strength and direction of monotonic associations between paired data. This nonparametric test was chosen due to its robustness against outliers and its capability to detect nonlinear relationships. Calculations were performed using the cor.test() function with the method set to SPEARMAN from the base R package.

Random forest prediction of traits in relation to the climate of origin

Utilizing the Random Forest (RF) package in R, we implemented a RF regression model to analyze the impact of climate on INT trait values under drought conditions, informed by 19 WorldClim Bioclimatic variables. Our models, each comprising 500 trees, were validated to ensure convergence, confirming that additional trees would not enhance predictive accuracy. The model's efficacy was assessed by comparing observed and predicted trait values. We then plotted the predicted values from the resulting RF model for traits across the range of *P. trichocarpa* to visualize the geographical patterns of traits and climate (Fig. 3b).

Genome-wide association studies (GWAS) Trait values and genotype means were transformed using a rank-based inverse normal transformation (INT) following Auer *et al.* (2016). This transformation standardizes genotype values to improve normality, reducing skewness and enhancing both statistical power and interpretability for downstream analyses. Genome-wide associations were conducted for all traits using genotype means for drought, control treatments, and their plasticity. Genomic variation, including SNPs and small insertions/deletions (InDels), was

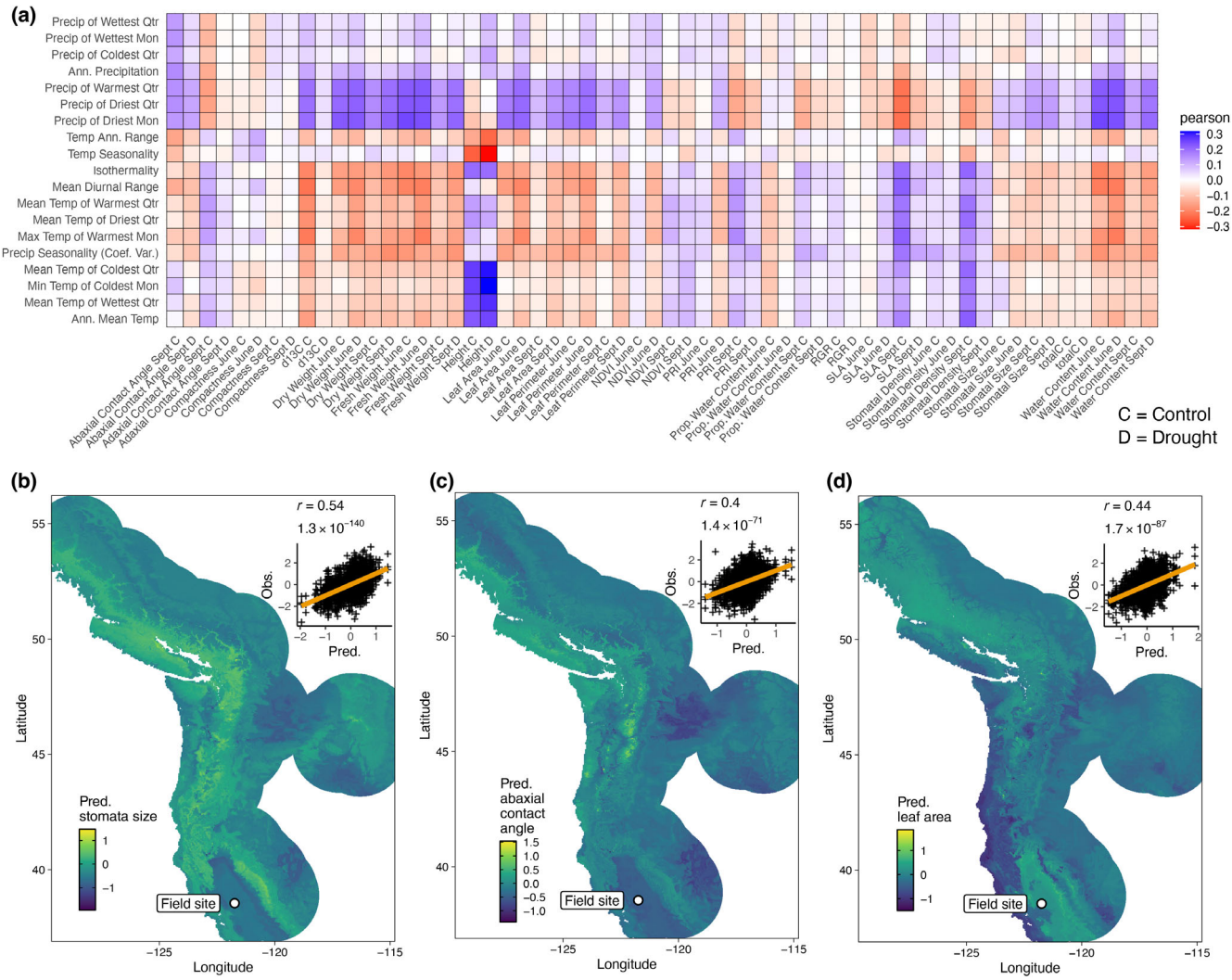

Fig. 3 Analyses of traits in relation to the climate-of-origin among *Populus trichocarpa* genotypes. (a) Heatmap illustrating Pearson correlations between stomatal traits and bioclimatic variables sourced from WorldClim. (b–d) Geographic distribution of predicted (b) stomatal size, (c) abaxial contact angle, and (d) leaf area based on Random Forest models, with scatterplot inset contrasting predicted vs observed values.

obtained from previous research (Tuskan *et al.*, 2006; Evans *et al.*, 2014). Associations between genome-wide genetic variants and phenotypic traits were analyzed using GEMMA (v.0.98.4) (Zhou & Stephens, 2012), incorporating a kinship matrix as a random covariate to account for population structure. Each genetic variant was modeled using the equation $\boldsymbol{y} = \boldsymbol{X\beta} + \boldsymbol{g} + \boldsymbol{\varepsilon}$, where $\boldsymbol{y}$ is the vector of trait values for each individual, $\boldsymbol{X}$ is the matrix of fixed effects (variants), $\boldsymbol{\beta}$ is the vector of fixed-effect coefficients, g represents the random genetic effect due to population structure and relatedness, and $\boldsymbol{\varepsilon}$ is the vector of residual errors. The statistical significance of allele–trait associations was determined by the *P*-value of $\boldsymbol{\beta}$. Variants were filtered to include only those with a minor allele frequency (MAF) ≥ 0.05. To identify putative GWAS peaks and address redundancies caused by linkage disequilibrium (LD), alleles were clustered using PLINK with parameters: --clump-p1 1, --clump-p2 1, --clump-r2 0.05, and --clump-kb 50. The 50-kb clumping threshold was informed by the genome-wide LD decay rate, which reached equilibrium at an r^2 of 0.05 within a 50-kb window. This process identified the most statistically significant allele for each LD group.

For visualization, clumped alleles were initially filtered to retain those with $P < 1 \times 10^{-4}$. Further refinement was performed based on a Bonferroni-corrected significance threshold ($P \leq 0.05$) using a chi-squared test to evaluate the significance of all linked alleles within each clump against a uniform *P*-value distribution. Genes located within 20 kb of the most significant variant in each clump were selected for downstream analyses (Figs 4, S5; Table S6). We visually inspected QQ plots to confirm adequate control for population structure (Fig. S6).

Putative paralogs of *Arabidopsis thaliana* genes (TAIR10) in the *P. trichocarpa* proteome were identified using BLASTP (BLAST v.2.13.0+) with the following criteria: E-value $< 1 \times 10^{-5}$, bitscore > 100, and percent identity $> 30\%$. For each *P. trichocarpa* protein, the *A. thaliana* gene with the lowest E-value was retained. We then checked the gene descriptions and gene ontology annotations for terms such as 'stomata', 'water', 'guard cell',

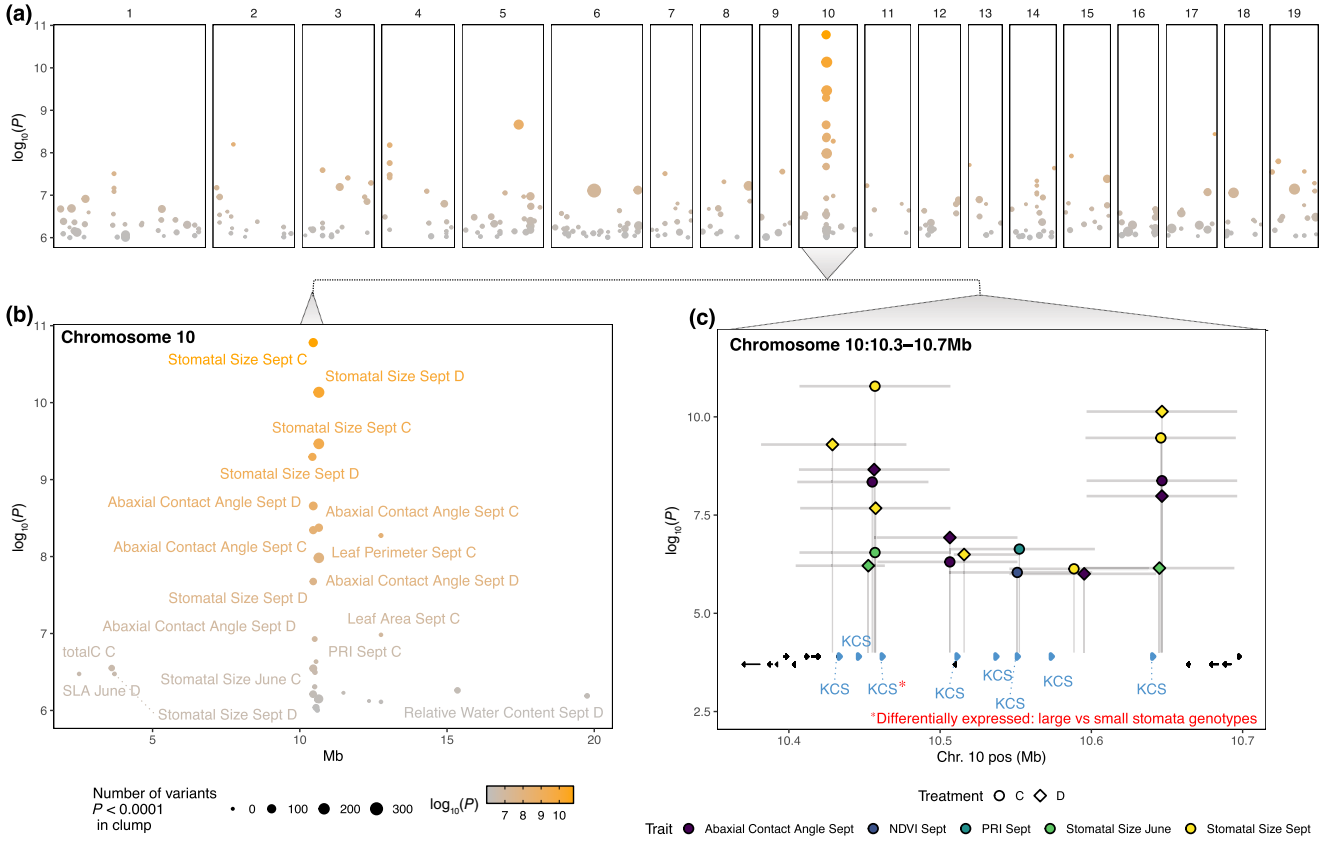

Fig. 4 Genome-wide association study (GWAS) reveals locus contributing to stomatal size. (a) Summary of GWAS across all traits. Points indicate the positions of clumps identified along the *Populus trichocarpa* genome. The color and size of points reflect the legend in (b). (b) A zoomed-in view of chromosome 10. (c) High-resolution view of a specific genomic region on chromosome 10, focusing on the interval containing significant clumps. Annotated genes within this region are highlighted, with KCS genes denoted by green. Vertical lines show the positions and significance of clumps for associations with specific traits. Horizontal lines indicate the range of variance within each clump.

and 'abscisic acid' to identify candidate genes associated with these processes. From this, we generated lists of loci (available in Table S7) for future research aimed at identifying potential causal loci. The number of times each gene was located within 20 kb of a GWAS signal associated with traits was also recorded to guide further exploration.

Elucidating the role of chromosome 10 locus in stomatal size

We examined, in greater detail, a locus on chromosome 10 consistently associated with stomatal size under both drought and control treatments and at two measurement time points (Fig. S7). The pronounced signal from this locus provided a unique opportunity for an in-depth case study, aiming to answer several pivotal questions:

To assess the LD across this genomic window, we calculated the Pearson correlation between all variant pairs in this 20 kb window, subsequently visualizing the results in a heatmap format and by visualizing LD with the most significant variant. Utilizing a RF model (implemented in R using the randomForest package, with 500 trees), we modeled trait–climate relationships based on genotypes with known phenotypic data. This model enabled us to predict stomatal size for genotypes with previously unmeasured traits based on their climate of origin, employing bioclimatic variables sourced from WorldClim v.2.0. We then assessed the predicted allele effects by examining these predicted phenotypes with the respective allele states across our dataset.

Lastly, we investigated the relationship between allele state and climatic variables. This entailed calculating the *t*-statistic for the correlation between allele states and each individual bioclimatic variable. Furthermore, we employed a RF model, incorporating all bioclimatic variables, to predict allele states. The accuracy of this model was gauged through analysis of the confusion matrix in R. Predicted allele states were projected and mapped across the geographical range of *P. trichocarpa* (Fig. S8).

Future climate predictions of chromosome 10 locus

To investigate the potential impact of future climate changes on the frequency of a specific allele associated with stomatal size on chromosome 10, we employed high-resolution future climate projections and predictive modeling. This allele was selected

based on its significant association with stomatal size and the climate of origin, suggesting its potential responsiveness to future climatic shifts. We utilized downscaled future climate projections (10-min spatial resolution) from the Coupled Model Intercomparison Project Phase 6 (CMIP6), available through WorldClim v.2.1, which, as described (https://www.worldclim.org/data/cmip6/cmip6climate.html), underwent both downscaling and calibration (bias correction) against the baseline climate provided by WorldClim v.2.1 Our analysis encompassed data from 10 global climate models (GCMs), specifically: ACCESS-CM2, CMCC-ESM2, EC-Earth3-Veg, GISS-E2-1-G, INM-CM5-0, IPSL-CM6A-LR, MIROC6, MPI-ESM1-2-HR, MRI-ESM2-0, and UKESM1-0-LL. We evaluated these models across four Shared Socio-economic Pathways (SSPs): SSP1-2.6, SSP2-4.5, SSP3-7.0, and SSP5-8.5, at four future time intervals: 2021–2040, 2041–2060, 2061–2080, and 2081–2100.

Initially, we compared future climate predictions to current climatic conditions (baseline) using bioclimatic variables from WorldClim, the geographic locations of *P. trichocarpa* genotypes. We performed *t*-tests, using the *t*-test statistic as a unitless measure of the severity of change for each bioclimatic variable. This preliminary step established an understanding of the extent of future climatic changes potentially facing *P. trichocarpa*.

To predict future allele frequencies, we adopted a machine learning approach using RF models in R. This involved analyzing the SNP with the strongest correlation to stomatal size within the identified locus on chromosome 10. Given the imbalanced genotype frequencies, we first balanced the dataset through random downsampling. From this balanced dataset, we trained a RF model to predict genotype frequencies based on bioclimatic variables. This model was applied to both the current climate baseline and all future climate scenarios for each combination of GCM, SSP, and time interval.

To ensure robustness, this process was iterated 100 times with random downsampling to obtain balanced training datasets, resulting in a total of 16 000 model predictions. For each prediction, we calculated the frequency of the allele associated with smaller stomata and compared it to the baseline frequency predicted from current climate conditions (Fig. 5).

RNA-Seq data generation and differential expression analysis

RNA extraction, library construction, and sequencing were conducted following the protocols described by Zhang *et al.* (2018). Sequencing was performed on the Illumina HiSeq 2500 platform using paired-end 150-bp reads. The dataset, including NCBI SRA accession numbers for publicly available sequences, is detailed in Tables S8 and S9.

Differential expression analysis was conducted to identify genes associated with stomatal size by comparing genotypes within the top 10% ('big' stomata) and bottom 10% ('small' stomata) quantiles. Raw RNA-Seq count data were processed using DESeq2 (Love *et al.*, 2014) in R. Genes with low expression (total counts ≤ 1 across all samples) were filtered out to enhance statistical power.

Significantly differentially expressed genes (DEGs) were identified using an adjusted *P*-value (P_{adj}) ≤ 0.05 and an absolute $\log_2$ fold change ($|\log_2 FC| \geq 1$. Gene annotations were integrated by mapping significant DEGs to the *Populus trichocarpa* genome (v.3.1) for functional insights. Results were visualized using volcano plots generated with ggplot2, highlighting the relationship between fold changes and statistical significance.

Results

Drought implementation and trait responses

We imposed drought and irrigated treatments on field trials of diverse *P. trichocarpa* during the summer of 2021 in Davis, CA (Figs 1, S1). The successful implementation of water limitation was confirmed by regular measurements of soil water potential and the lack of precipitation during the treatment period (Fig. S1). Total precipitation recorded from June to September 2021 was 0.51 mm. The effect of water deficit was visually evident in *P. trichocarpa* trees, such as wilting or yellowing leaves and early leaf shedding in the drought-treated trees. The effect of drought relative to control conditions was detected in a number of traits measured (Tables S1, S2, S3, S5), especially those traits related to biomass and performance. Drought treatment significantly reduced leaf size, leaf mass, height, and growth rate (Figs 2, 3). Among leaf morphological traits, we saw a significant trend for smaller, more dense stomata under drought conditions along with reductions in SLA, leaf perimeter, and abaxial contact angle, reflecting constraints on growth, and whether the plasticity is adaptive remains a question for future work (Figs 2, 3). Notably, water-related traits, such as $\delta^{13}C$, a proxy for WUE, were significantly higher under drought, suggesting a water-conservation response. For traits where measurements were made at multiple time points, the effect of drought was more pronounced on measurements made in September, after several months of water deficit, than in June, shortly after the onset of the drought treatment (Figs 2, 3). This is especially clear in spectral reflectance data. For example, the difference between control and drought for PRI and NDVI was most evident in September. In particular, PRI was dramatically reduced in drought-treated plants, indicative of physiological stress (Magney *et al.*, 2016; Wong *et al.*, 2022; Mulero *et al.*, 2023).

Trait correlations were similar under drought and control treatments (Fig. S4). Positive correlations were observed between stomatal size in June and stomatal size in September, indicating consistency in trait behavior across different growth stages and durations of drought (June vs September). A negative correlation was evident between stomatal density and stomatal size, consistent with previous observations in poplar (McKown *et al.*, 2014a) and other species (Franks *et al.*, 2009; Liu *et al.*, 2021). We also observed significant plasticity in several traits. The variance components analysis from the experimental field trial delineated variability in plant traits into three sources: Genotype (G), Treatment (T), and their interaction (G × T). Genotypic variance was observed across most traits, underscoring the significance of genetic differences among the samples

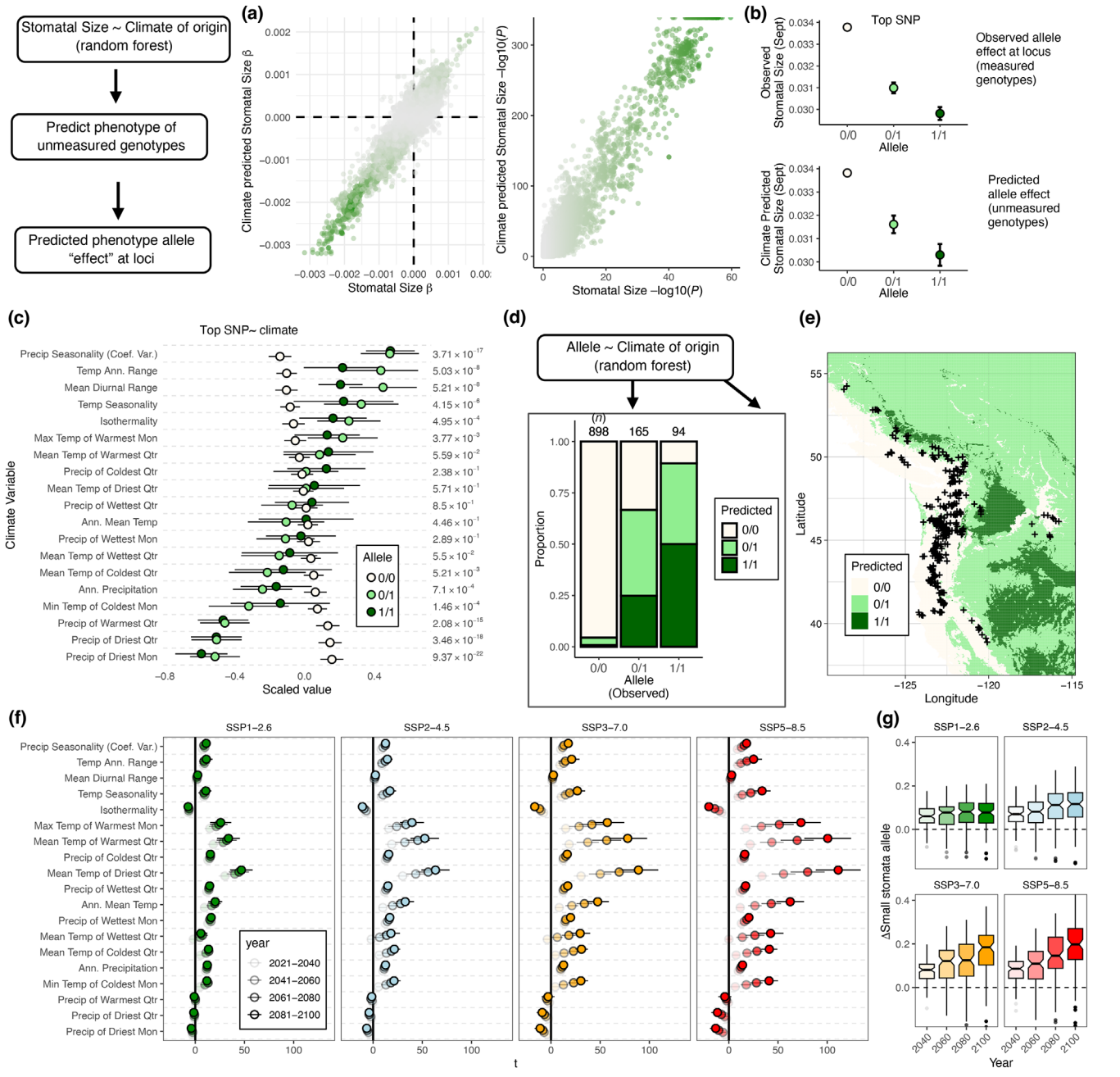

Fig. 5 Analysis of locus on chromosome 10 (10 356 950–10 746 695) associated with stomatal size in *Populus trichocarpa*. (a) Left: allele effects on stomatal size (left: β, right: $-\log_{10}(P)$) from simple linear regression phenotype–allele across all observations and 'allele effects' on climate-predicted allele effects of genotypes with unmeasured phenotypes in the region on chromosome 10. (b) Depiction of allele effect on stomatal size for genotypes with measured (upper) and climate-predicted (lower) phenotypes. Each point illustrates the mean, while error bars (barely visible) represent ± 2 SE. (c) T-statistic values from Pearson correlation, illustrating the relationship between allele state and the climate origin of genotypes. (d) Visualization of the prediction accuracy of the Random Forest model, presenting the proportion of predicted allele states corresponding to each observed allele. (e) Geographical mapping of predicted allele states based on bioclimatic variables. (f) Change in bioclimatic variables from historical measures under various climate scenarios (SSPs and time). *x*-axis (T) represents the *t*-test difference between future and current measures. Points mark mean values, where error bars indicate SE across 10 global climate models (GCMs). (g) Predicted change in frequency of small stomata allele on chromosome 10 under future climates. Boxplots represent predictions averaged across GCMs for 100 iterations of randomized, balanced training sets for Random Forest models of genotype–bioclimatic variables under contemporary climates, used to predict genotype states in *P. trichocarpa*.

(Fig. S2). Environmental treatments significantly affected traits such as stomatal size in September and leaf compactness in June. The interaction between genotype and treatment was evident in traits such as water content, indicating a differential response of genotypes to various treatments. Overall, the findings emphasize the complex interplay of genetics and environment in

determining plant trait variability, in particular, in response to drought.

For the drought treatment, where replication allowed such analyses (see Materials and Methods section), all traits showed significant clonal repeatability (H2R) except for adaxial contact angle, a proxy for wettability, for the time point measured in September (Fig. S3a). As expected, we observed high genetic correlation (rG) for traits across June and September (Fig. S3b). Leaf biomass traits (perimeter, dry, and fresh weight) showed high positive rG with each other and were significantly negatively correlated with SLA. Interestingly, rG was strongly negative between adaxial and abaxial contact angles, indicating possible trade-offs between these traits. Furthermore, adaxial contact angle was strongly negatively correlated with leaf biomass traits, relative water content, RGR, NDVI, and PRI. As also seen with phenotypic correlations, stomatal density and stomatal size showed strong negative rG.

Relationships between traits and climatic conditions

We found significant correlations between plant traits and the climate of their origin (Fig. 3). Greater leaf size and weight, for instance, were predominantly associated with cooler, wetter climates. Notably, stomatal density and size demonstrated contrasting relationships to climatic conditions. Specifically, genotypes originating from warmer, arid climates exhibited higher stomatal densities but possessed smaller stomatal sizes. Warmer, drier climates correlated with less negative $\delta^{13}C$ (WUE) values. To provide a more nuanced understanding of the interaction between climatic variables and plant phenotypes, we employed RF models (Fig. 3b–d). The strength of RF models lies in their ability to detect nonlinearities and interactions, thereby potentially enhancing the accuracy of predictions. Nevertheless, they do present challenges in terms of interpretability for targeted hypothesis testing. These RF models confirmed a marked correlation between the predicted values and the actual measurements. Visualizing these predictions across the range further emphasized the relationships between stomatal size, geography, and climate.

Genome-wide associations (GWAS)

We performed GWAS analyses for each trait: phenotypes under drought, control, and the difference (plasticity) (Figs 5, S5–S7; Tables S5, S6). These analyses identified loci explaining variance in traits after accounting for population structure. In total, across all traits, environments, and plasticity, we identified 303 significant associations, each reflecting a cluster of SNP variants in LD enriched for association with the trait of interest.

Evaluating GWAS results across traits after variant clumping and considering multiple testing revealed a notable locus on chromosome 10. This region was significantly associated with stomatal size in both drought and control treatments, and for measurements in both June and September, as well as for abaxial contact angle, a proxy measure of cuticle wax (Figs 4, S6, S7). We found that alleles in this locus explained 15.9% of the variance in stomatal size across all measured plants, irrespective of treatment. This region contains a cassette of tandem 3-ketoacyl-CoA synthase (KCS) family genes, with KCS genes being previously linked to both cuticular wax and stomatal traits (Gray *et al.*, 2000; Gonzales-Vigil *et al.*, 2017). A KCS gene in this region was previously linked to high alkene content in abaxial cuticular wax and differences in stomatal size in *P. trichocarpa* (Gonzales-Vigil *et al.*, 2017), and may also be linked to *Melampsora* and *Septoria* resistance (pers. comm). The LD around this region revealed that the variants with strong associations had significant long-range LD with one another, consistent with a solitary causal locus with extensive LD with neighboring variants (Fig. S7).

For more mechanistic insight into variation in stomata size, we used a bulk segregant RNA-Seq analysis from leaf tissue (Table 8). We identified 51 genes differentially expressed between the top and bottom deciles of genotypes ranked by stomata size. Only one of these genes colocalized with a GWAS signal: Potri.010G079500, which showed a >4-fold difference in expression ($P = 7.35 \times 10^{-5}$, $P_{adj} = 0.046$), one of the KCS genes on chromosome 10 adjacent to the most significant GWAS signal for stomata size (Fig. 4c), providing further evidence for the causal link between variation in KCS genes and stomatal size.

To explore its role in local adaptation to climate, we estimated allele effects on climate-predicted phenotypes for *P. trichocarpa* genotypes whose stomatal phenotypes were not analyzed in this study (Fig. 5). The rationale behind this approach was multifold. Primarily, it served as a strategy to verify the integrity of climate–trait associations. If the phenotype predictions based on climate were accurate and reflected local adaptation, they should replicate the empirical allele effects observed in genotypes for which phenotypes were measured. Second, it showcases the potential of leveraging local adaptation in employing climate-predicted phenotypes in a broader genotype sample to augment efforts in pinpointing physiologically significant loci. These analyses are, in essence, a form of environmental GWAS that treats the environment of origin as a phenotype (e.g. Ferrero-Serrano & Assmann, 2019). In our case, because the predicted phenotype is derived entirely from the climate of origin, it reflects a transformation of the environmental parameters fit to a target trait, thereby potentially enhancing the study of locally adaptive alleles.

These analyses confirmed that observed allele effects were highly predictive of allele effects on phenotypes predicted by climate of origin in unmeasured genotypes (stomatal size: $r = 0.95$, $P < 2 \times 10^{-16}$). Examining the most significant SNP within this region yielded two noteworthy findings: an observable additive effect where heterozygous individuals presented an intermediate phenotype and a match between the empirical 'effect' and climate-predicted phenotypes (Fig. 5). Further exploration into climate–allele associations revealed that alleles linked with small stomata were predominant in environments characterized by reduced warm-season precipitation and greater precipitation seasonality (Figs 5d, S8). This aligns with the general trait correlations we noted, consistent with the distribution of alleles at this locus reflecting local adaptation to climate. The robustness of the relationship between the climate and allele state is further

emphasized when predicting the allele state using the RF model based on climate parameters (χ^2 test, $P < 2 \times 10^{-16}$, Fig. 5).

Future climates

Given the strong link between loci affecting stomata size and climate, we set out to ask whether this yields predictions about future evolution at this locus. We evaluated the severity of climate change across various bioclimatic variables at the geographic locations of *P. trichocarpa*. These were based on different SSPs and temporal projections, revealing that more intense SSP scenarios forecasted more substantial changes in climate, intensifying over time (Fig. 5g,i).

As expected, the predicted changes in climate suggest a general trend toward warming. Notably, there is an expected increase in the extremities of precipitation – wetter conditions during the colder months, coupled with drier conditions throughout the summer months. These shifts in temperature and precipitation patterns may drive natural selection on stomatal size. The allele associated with smaller stomatal size is found to be more prevalent in environments with high intra-annual precipitation variability and drier summer months – conditions that are expected to become more common in the future for *P. trichocarpa* (Fig. 5g,h).

Our predictive models, averaging across all 10 GCMs for each set of 100 random iterations, indicated a predicted increase in the expected frequency of the small stomata allele, particularly under the more severe climate scenarios (SSP3-7.0 and SSP5-8.5), with a notable escalation over time (Fig. 5g,h). These increments were most pronounced in the latter half of the 21st century. Taken together, these findings support the hypothesis that allelic variation associated with stomatal size reflects local adaptation to climate, which may be perturbed by extreme climate change.

Discussion

This study has identified novel genetic loci that underpin phenotypic variation in stomatal and other leaf traits linked to *P. trichocarpa* crop adaptation to future water-limited environments. These findings will be informative in enabling future feedstock development for marginal environments. By deploying a controlled drought experiment, subjecting over 7000 trees across 6.1 ha to a controlled soil moisture deficit, we have begun to unravel the complexities of adaptive vs plastic responses to drought. Our findings provide evidence for local adaptation in *P. trichocarpa*, with associations between climate and functional traits (Viger *et al.*, 2016).

We estimated the genetic variance of drought-related traits using broad-sense heritability (H2R), an upper-limit estimate of the proportion of total genetic variance to phenotypic variance. Control block estimates were not possible due to single ramet measurements per genet. SNP-heritability results were similar to H2R, suggesting overestimation of additive genetic values, likely due to low relatedness among genets causing the genomic relationship matrix to approximate an identity matrix. While we could not fully separate additive from nonadditive genetic effects, estimates of genetic correlations (rG) provided key insights.

Stomatal size and density showed high heritability and a strong negative genetic correlation, consistent with their functional trade-off under WUE constraints. This trade-off has been observed across other tree species and validated through genetic manipulation in Arabidopsis. Leaf traits like PRI and NDVI, which are indicative of light absorption processes, also showed strong negative genetic correlations with adaxial contact angle and most leaf biomass traits. Lower adaxial contact angle indicates increased wettability, which could reduce gas exchange and carbon assimilation. These observed correlations suggest that leaf morphology and associated indices may reflect adaptive mechanisms under drought stress in our plantation setting.

Our analysis indicates that stomatal traits are closely linked to the climatic conditions of their geographic origin, with genotypes from hotter, drier climates often exhibiting smaller, denser stomata, consistent with previous findings (Pearce *et al.*, 2006). This relationship is valuable for considering poplar as a bioenergy crop in marginal lands and could help inform the selection of genotypes with stomatal traits and other traits aligned to the target environment of production. The plastic response of stomatal size reduction under drought conditions may reflect an adaptive response, supporting smaller stomata associated with arid environments and underscoring their role in optimizing WUE (Dunlap & Stettler, 2001). No strong relationship between stomatal size and height or RGR (Fig. S4) was observed, indicating that these traits can be disentangled, enabling future selection and breeding of adaptive stomatal traits for hot and dry environments, with maintained yield. While WUE increased under drought, potentially reflecting adaptive plasticity, a relationship with stomata size was not evident.

We identified a significant locus on chromosome 10 associated with stomatal size and abaxial contact angle, showing a distribution among genotypes highly predicted by the climate of origin. A significant locus on chromosome 10 was previously found to be important in determining $\delta^{13}C$ in a biparental mapping population with one grandparent as *P. trichocarpa* (Viger *et al.*, 2013), thus linked to plant WUE. Of the known candidates that map to this chromosome 10 locus, 3-ketoacyl-CoA synthase 11, KCS11 is a gene family member involved in the biosynthesis of very long chain fatty acids codes for long-chain fatty acids, already shown to have a role in stomatal development and function in relation to drought tolerance and stomatal response to elevated carbon dioxide (Gray *et al.*, 2000; Tang *et al.*, 2020). Future work will benefit from the availability of long-read sequence data to capture potential structural variants and long-range haplotypes that characterize the variation in this region for greater causal inference. This could prove a promising candidate for genetic exploration to enable precise gene editing (Allwright & Taylor, 2016; Taylor *et al.*, 2019, 2024). Investigating this and other loci could reveal causal variants, providing breeders with tools to develop *Populus* varieties tailored for specific environmental demands. This approach aligns with sustainable biofuel production goals and broader environmental stewardship efforts. However, detailed mapping of these regions is necessary to unravel underlying

genetic mechanisms (Table S7). Presently, these genetic markers identified provide a resource for future studies aiming to dissect the genetic basis of adaptation in *P. trichocarpa*.

P. trichocarpa's current adaptation to its climate underlines the need to explore resilience under changing future climates, since the ability to predict alleles with future adaptive value is essential for conservation and the management of natural populations (Blumstein *et al.*, 2020). The adaptability shown by *Populus balsamifera*, through a wide range of adaptive physiological responses, offers hope for potential resilience against future climate shifts (Keller *et al.*, 2011). The clinal variation and genomic signals observed in *P. trichocarpa* indicate a blend of unique and shared adaptive responses to different environmental gradients, shaped by genomic, environmental, and functional factors (Zhang *et al.*, 2019). Such insights lay the groundwork for understanding adaptation mechanisms in species facing climate change threats.

Predicting stomatal size from the climate of origin offers an approach to inferring phenotype values in genotypes without direct measurements, aiding in the association between observed alleles and traits. This methodology holds potential for streamlining the assessment of complex physiological traits, though its applicability across various traits and species requires more empirical validation. We found novel evidence of predicted allele frequency shifts toward those associated with smaller stomatal size under future climate projections, especially under severe scenarios, suggesting that natural selection may favor traits conducive to surviving anticipated shifts in precipitation patterns (Fig. 5). This trend prompts crucial considerations about the pace of evolutionary dynamics in perennial species like *P. trichocarpa* in response to forecasted rapid environmental changes and the implications for the species' persistence and resilience. By contrast, for research on conifer trees, there is evidence of limited adaptation to local climate for populations of Douglas-fir (Candido-Ribeiro & Aitken, 2024). Although this study largely considered photosynthetic traits only and is in contrast to earlier research on Douglas-fir, that demonstrated significant intraspecific population variation in traits in relation to the climate of origin (Bansal *et al.*, 2015), or relevance to identifying adaptive and plastic responses to enable drought tolerance in the face of climate change. For *P. trichocarpa*, our data suggest a significant need for allele frequency shifts with climate, but the timing and importance of these phenomena require further investigation.

While our findings provide valuable insights into loci and traits associated with drought tolerance, it is critical to acknowledge the inherent trade-off between drought tolerance and yield. Resources allocated to survival mechanisms under stress conditions often come at the expense of growth performance, particularly over multiple years. Breeding strategies must carefully navigate this balance to develop genotypes capable of both surviving extreme conditions and maintaining productivity. The loci identified in this study offer a promising foundation for achieving this balance, but long-term evaluations under variable environmental conditions are needed to fully understand their implications.

Utilizing natural populations preserves biodiversity and reduces the long breeding cycles typical of forest trees by maintaining allele–phenotype relationships. While marker-assisted selection often struggles with complex traits, genomic selection, leveraging genome-wide markers to predict traits beyond known climatic envelopes, offers significant potential for adaptive breeding strategies under climate change (Grattapaglia *et al.*, 2018; Cortés *et al.*, 2020; Depardieu *et al.*, 2020). Additionally, our research supports identifying single gene targets for gene editing, as demonstrated in *Populus* (Zhou *et al.*, 2015), accelerating wood domestication (Anders *et al.*, 2023).

Poplar is a fast-growing, short-rotation crop with diverse applications, including the production of Sustainable Aviation Fuel (SAF) (Webber *et al.*, 2024), BECCS, and other bio-based uses, making it a cornerstone of sustainable energy strategies (Sannigrahi *et al.*, 2010; Porth & El-Kassaby, 2015). This versatility emphasizes the importance of breeding programs aimed at improving efficiency, yield, and adaptability, particularly on marginal, water-limited sites–a key limitation for bioenergy crop deployment (King *et al.*, 2013). Together, these approaches can optimize woody feedstocks for future climates while addressing the critical trade-offs between drought tolerance and yield. This aligns with the U.S. Department of Energy's goals to triple biomass supply and meet 15% of energy demand through sustainable bioenergy crops (U.S. Department of Energy, 2024). By addressing these gaps, our work advances conservation and breeding strategies for poplar and other species, supporting its diverse applications in a changing global climate.

Conclusions

We have uncovered evidence of adaptive variation in stomatal and leaf traits within *P. trichocarpa*, pinpointing a set of loci associated with genetic variation under both drought and control conditions, as well as their plasticity. Our findings also underscore the critical role of climate in shaping the adaptive landscape of *P. trichocarpa*, casting light on potential challenges and opportunities for this species in the face of climate change. Leveraging climate-predicted phenotypes provided compelling evidence for the adaptive significance of a locus associated with stomata size, which is predicted to respond to selection under future climates. In summary, this work offers pivotal insights into the intricate genetic underpinnings of physiological traits and their drought responses in *P. trichocarpa*, with implications for both conservation strategies and breeding initiatives.

Acknowledgements

This material is based on work supported by the Center for Bioenergy Innovation (CBI), U.S. Department of Energy, Office of Science, Biological and Environmental Research Program under Award No. ERKP886. Research in the laboratory of Gail Taylor is supported by the John B. Orr endowment in Environmental Plant Sciences, and this project was supported by the Genomics-Enabled Plant Biology for Determination of Gene Function program by the Office of Biological and Environmental Research in

the DOE Office of Science (Award DE-SC0020164). MCK acknowledges the Department of Plant Sciences, UC Davis, for the award of a GSR scholarship funded by endowments, particularly the James Monroe McDonald Endowment, administered by UCANR. We thank all UC Davis interns, graduate students, and postdocs who helped with field collections and lab assistance on this project. This paper is dedicated to the memory of our wonderful colleague and friend, Dr Wellington Muchero, who is much missed.

Competing interests

None declared.

Author contributions

GT, JGC, TT, GAT and WM conceptualized the study. GT, ZM, JGC, TT, JBB, SM, MCK and WM designed the methodology. MK, PS, JL, MS, CRA, JGM, HC, COB and ML performed the formal analysis. GT, JGC, TT, ZM, JBB, MK, PFS and WM carried out the investigation. GT, JGC, GAT and TT provided the resources. GT, MK, JBB, ZM, WM, PFS and SM curated the data. MK and GT wrote the original manuscript draft. All authors reviewed and edited the manuscript. GT, TSM and TNB supervised the study. GT handled project administration. GT, JGC and TT secured funding for the project.

ORCID

Chanaka Roshan Abeyratne https://orcid.org/0000-0002-9561-3955
Jack Bailey-Bale https://orcid.org/0009-0007-3816-6531
Thomas N. Buckley https://orcid.org/0000-0001-7610-7136
Jin-Gui Chen https://orcid.org/0000-0002-1752-4201
Hari Chhetri https://orcid.org/0000-0001-6820-8789
Peter Freer-Smith https://orcid.org/0000-0002-4465-1927
Marie C. Klein https://orcid.org/0009-0003-4199-8970
John Lagergren https://orcid.org/0000-0002-8092-7433
Matthew Lane https://orcid.org/0000-0002-7750-6822
Troy S. Magney https://orcid.org/0000-0002-9033-0024
J. Grey Monroe https://orcid.org/0000-0002-4025-5572
Wellington Muchero https://orcid.org/0000-0002-0200-9856
Mengjun Shu https://orcid.org/0000-0002-6323-2664
Gail Taylor https://orcid.org/0000-0001-8470-6390
Timothy J. Tschaplinski https://orcid.org/0000-0002-9540-6622
Gerald A. Tuskan https://orcid.org/0000-0003-0106-1289

Data availability

All data supporting the findings of this study are available within the article and its Supporting Information. Raw phenotypic data and GWAS summary statistics are provided in Supporting Information Tables S1 and S2, respectively. Additional methodological details are available in the Materials and Methods section and Supporting Information Figs S1–S5. Genotypic data were based on the *Populus trichocarpa* genome v.4.1 (Phytozome genome ID: 533).

References

Allwright MR, Taylor G. 2016. Molecular breeding for improved second generation bioenergy crops. *Trends in Plant Science* **21**: 43–54.

Anders C, Hoengenaert L, Boerjan W. 2023. Accelerating wood domestication in forest trees through genome editing: advances and prospects. *Current Opinion in Plant Biology* **71**: 102329.

Aparecido LMT, Miller GR, Cahill AT, Moore GW. 2017. Leaf surface traits and water storage retention affect photosynthetic responses to leaf surface wetness among wet tropical forest and semiarid savanna plants. *Tree Physiology* **37**: 1285–1300.

Apuli R-P, Richards T, Rendón-Anaya M, Karacic A, Rönnberg-Wästljung A-C, Ingvarsson PK. 2021. The genetic basis of adaptation in phenology in an introduced population of Black Cottonwood (*Populus trichocarpa*, Torr. & Gray). *BMC Plant Biology* **21**: 317.

Auer P, Reiner A, Leal S. 2016. The effect of phenotypic outliers and non-normality on rare-variant association testing. *European Journal of Human Genetics* **24**: 1188–1194.

Bansal S, Harrington CA, Gould PJ, St Clair JB. 2015. Climate-related genetic variation in drought-resistance of Douglas-fir (*Pseudotsuga menziesii*). *Global Change Biology* **21**: 947–958.

Beerling DJ, Woodward FI. 2008. Changes in land plant function over the Phanerozoic: reconstructions based on the fossil record. *Botanical Journal of the Linnean Society* **124**: 137–153.

Benavides R, Carvalho B, Bastias CC, López-Quiroga D, Mas A, Cavers S, Gray A, Albet A, Alía R, Ambrosio O *et al.* 2021. The GenTree Leaf Collection: inter- and intraspecific leaf variation in seven forest tree species in Europe. *Global Ecology and Biogeography* **30**: 590–597.

Blumstein M, Richardson A, Weston D, Zhang J, Muchero W, Hopkins R. 2020. A new perspective on ecological prediction reveals limits to climate adaptation in a temperate tree species. *Current Biology: CB* **30**: 1447–1453.

Bogeat-Triboulot MB, Buré C, Gerardin T, Chuste PA, Le Thiec D, Hummel I, Durand M, Wildhagen H, Douthe C, Molins A *et al.* 2019. Additive effects of high growth rate and low transpiration rate drive differences in whole plant transpiration efficiency among black poplar genotypes. *Environmental and Experimental Botany* **166**: 103784.

Brosché M, Vinocur B, Alatalo ER, Lamminmäki A, Teichmann T, Ottow EA, Djilianov D, Afif D, Bogeat-Triboulot M-B, Altman A *et al.* 2005. Gene expression and metabolite profiling of *Populus euphratica* growing in the Negev desert. *Genome Biology* **6**: R101.

Candido-Ribeiro R, Aitken SN. 2024. Weak local adaptation to drought in seedlings of a widespread conifer. *New Phytologist* **241**: 2395–2409.

Cavallaro A, Carbonell-Silletta L, Burek A, Goldstein G, Scholz FG, Bucci SJ. 2022. Leaf surface traits contributing to wettability, water interception and uptake of above-ground water sources in shrubs of Patagonian arid ecosystems. *Annals of Botany* **130**: 409–418.

Clifton-Brown J, Harfouche A, Casler MD, Dylan Jones H, Macalpine WJ, Murphy-Bokern D, Smart LB, Adler A, Ashman C, Awty-Carroll D *et al.* 2019. Breeding progress and preparedness for mass-scale deployment of perennial lignocellulosic biomass crops switchgrass, miscanthus, willow and poplar. *Global Change Biology. Bioenergy* **11**: 118–151.

Cocozza C, Cherubini P, Regier N, Saurer M, Frey B, Tognetti R. 2010. Early effects of water deficit on two parental clones of *Populus nigra* grown under different environmental conditions. *Functional Plant Biology* **37**: 244–254.

Cook BI, Mankin JS, Anchukaitis KJ. 2018. Climate change and drought: from past to future. *Current Climate Change Reports* **4**: 164–179.

Cortés AJ, Restrepo-Montoya M, Bedoya-Canas LE. 2020. Modern strategies to assess and breed forest tree adaptation to changing climate. *Frontiers in Plant Science* **11**: 583323.

Covarrubias-Pazaran G. 2016. Genome-assisted prediction of quantitative traits using the R package sommer. *PLoS ONE* **11**: e0156744.

Dai A. 2012. Increasing drought under global warming in observations and models. *Nature Climate Change* **3**: 52–58.

Depardieu C, Girardin MP, Nadeau S, Lenz P, Bousquet J, Isabel N. 2020. Adaptive genetic variation to drought in a widely distributed conifer suggests a potential for increasing forest resilience in a drying climate. *New Phytologist* **227**: 427–439.

Dittberner H, Korte A, Mettler-Altmann T. 2018. Natural variation in stomata size contributes to the local adaptation of water-use efficiency in Arabidopsis thaliana. *Molecular Ecology* **27**: 14838.

Doheny-Adams T, Hunt L, Franks PJ, Beerling DJ, Gray JE. 2012. Genetic manipulation of stomatal density influences stomatal size, plant growth and tolerance to restricted water supply across a growth carbon dioxide gradient. *Philosophical Transactions of the Royal Society of London. Series B, Biological Sciences* **367**: 547–555.

Dunlap JM, Stettler RF. 2001. Variation in leaf epidermal and stomatal traits of *Populus trichocarpafrom* two transects across the Washington Cascades. *Canadian Journal of Botany* **79**: 528–536.

Evans LM, Slavov GT, Rodgers-Melnick E, Martin J, Ranjan P, Muchero W, Brunner AM, Schackwitz W, Gunter L, Chen J-G *et al.* 2014. Population genomics of *Populus trichocarpa* identifies signatures of selection and adaptive trait associations. *Nature Genetics* **46**: 1089–1096.

Ferrero-Serrano Á, Assmann SM. 2019. Phenotypic and genome-wide association with the local environment of Arabidopsis. *Nature Ecology & Evolution* **3**: 274–285.

Fick SE, Hijmans RJ. 2017. WorldClim 2: new 1-km spatial resolution climate surfaces for global land areas. *International Journal of Climatology* **37**: 4302–4315.

Food and Agriculture Organization of the United Nations, United Nations International Children's Emergency Fund, World Health Organization, World Food Programme, International Fund for Agriculture Development. 2018. *The State of Food Security and Nutrition in the World 2018: Building climate resilience for food security and nutrition.* Rome, Italy: Food & Agriculture Org.

Franks PJ, Beerling DJ. 2009. Maximum leaf conductance driven by CO_2 effects on stomatal size and density over geologic time. *Proceedings of the National Academy of Sciences, USA* **106**: 10343–10347.

Franks PJ, Drake PL, Beerling DJ. 2009. Plasticity in maximum stomatal conductance constrained by negative correlation between stomatal size and density: an analysis usingEucalyptus globulus. *Plant, Cell & Environment* **32**: 1737–1748.

Gonzales-Vigil E, Hefer CA, von Loessl ME, La Mantia J, Mansfield SD. 2017. Exploiting natural variation to uncover an alkene biosynthetic enzyme in poplar. *Plant Cell* **29**: 2000–2015.

Gornall JL, Guy RD. 2007. Geographic variation in ecophysiological traits of black cottonwood (*Populus trichocarpa*). *Canadian Journal of Botany* **85**: 1202.

Grattapaglia D, Silva-Junior OB, Resende RT, Cappa EP, Müller BSF, Tan B, Isik F, Ratcliffe B, El-Kassaby YA. 2018. Quantitative genetics and genomics converge to accelerate forest tree breeding. *Frontiers in Plant Science* **9**: 1693.

Gray JE, Holroyd GH, van der Lee FM, Bahrami AR, Sijmons PC, Woodward FI, Schuch W, Hetherington AM. 2000. The HIC signalling pathway links CO_2 perception to stomatal development. *Nature* **408**: 713–716.

Hetherington AM, Woodward FI. 2003. The role of stomata in sensing and driving environmental change. *Nature* **424**: 901–908.

Hoegh-Guldberg O, Jacob D, Bindi M. 2018. Impacts of 1.5 C global warming on natural and human systems. *Global Warming* **20**: 11749.

Huang X, Xiao X, Zhang S, Korpelainen H, Li C. 2009. Leaf morphological and physiological responses to drought and shade in two *Populus cathayana* populations. *Biologia Plantarum* **53**: 588–592.

Kačík F, Ďurkovič J, Kačíková D. 2012. Chemical profiles of wood components of Poplar clones for their energy utilization. *Energies* **5**: 5243–5256.

Kardiman R, Ræbild A. 2018. Relationship between stomatal density, size and speed of opening in Sumatran rainforest species. *Tree Physiology* **38**: 696–705.

Keller SR, Soolanayakanahally RY, Guy RD, Silim SN, Olson MS, Tiffin P. 2011. Climate-driven local adaptation of ecophysiology and phenology in balsam poplar, *Populus balsamifera* L. (Salicaceae). *American Journal of Botany* **98**: 99–108.

King JS, Ceulemans R, Albaugh JM, Dillen SY, Domec J-C, Fichot R, Fischer M, Leggett Z, Sucre E, Trnka M *et al.* 2013. The challenge of lignocellulosic bioenergy in a water-limited world. *Bioscience* **63**: 102–117.

Kwon DH, Huh HK, Lee SJ. 2014. Wettability and impact dynamics of water droplets on rice (*Oryza sativa* L.) leaves. *Experiments in Fluids* **55**: 1691.

Lagergren J, Pavicic M, Chhetri HB, York LM, Hyatt PD, Kainer D, Rutter EM, Flores K, Bailey-Bale J, Klein M *et al.* 2023. Few-shot learning enables population-scale analysis of leaf traits in *Populus trichocarpa*. *Plant Phenomics* **5**: 10351.

Liu C, Muir CD, Li Y, Xu L, Li M, Zhang J, de Boer HJ, Sack L, Han X, Yu G *et al.* 2021. Scaling between stomatal size and density in forest plants. *bioRxiv*. doi: 10.1101/2021.04.25.441252.

Liu Z, Hikosaka K, Li F, Jin G. 2020. Variations in leaf economics spectrum traits for an evergreen coniferous species: tree size dominates over environment factors. *Functional Ecology* **34**: 458–467.

Love MI, Huber W, Anders S. 2014. Moderated estimation of fold change and dispersion for RNA-seq data with DESeq2. *Genome Biology* **15**: 550.

Lynch M, Walsh B. 1998. *Genetics and analysis of quantitative traits*. Oxford, UK: Oxford University Press.

Magney TS, Vierling LA, Eitel JUH, Huggins DR, Garrity SR. 2016. Response of high frequency Photochemical Reflectance Index (PRI) measurements to environmental conditions in wheat. *Remote Sensing of Environment* **173**: 84–97.

Marron N, Delay D, Petit J-M, Dreyer E, Kahlem G, Delmotte FM, Brignolas F. 2002. Physiological traits of two *Populus* × *euramericana* clones, Luisa Avanzo and Dorskamp, during a water stress and re-watering cycle. *Tree Physiology* **22**: 849–858.

McKown AD, Guy RD, Klápště J, Geraldes A, Friedmann M, Cronk QCB, El-Kassaby YA, Mansfield SD, Douglas CJ. 2014a. Geographical and environmental gradients shape phenotypic trait variation and genetic structure in *Populus trichocarpa*. *New Phytologist* **201**: 1263–1276.

McKown AD, Guy RD, Quamme L, Klápště J. 2014b. Association genetics, geography and ecophysiology link stomatal patterning in *Populus trichocarpa* with carbon gain and disease resistance trade-offs. *Molecular Ecology* **23**: 12969.

McKown AD, Klápště J, Guy RD, Corea ORA, Fritsche S, Ehlting J, El-Kassaby YA, Mansfield SD. 2019. A role for SPEECHLESS in the integration of leaf stomatal patterning with the growth vs disease trade-off in poplar. *New Phytologist* **223**: 1888–1903.

McKown AD, Klápště J, Guy RD, Geraldes A, Porth I, Hannemann J, Friedmann M, Muchero W, Tuskan GA, Ehlting J *et al.* 2014c. Genome-wide association implicates numerous genes underlying ecological trait variation in natural populations of *Populus trichocarpa*. *New Phytologist* **203**: 535–553.

Mehmood MA, Ibrahim M, Rashid U, Nawaz M, Ali S, Hussain A, Gull M. 2017. Biomass production for bioenergy using marginal lands. *Sustainable Production and Consumption* **9**: 3–21.

Moghaddam A, Raza A, Vollmann J, Ardakani MR, Wanek W, Gollner G, Friedel JK. 2013. Carbon isotope discrimination and water use efficiency relationships of alfalfa genotypes under irrigated and rain-fed organic farming. *European Journal of Agronomy* **50**: 82–89.

Monclus R, Dreyer E, Villar M, Delmotte FM, Delay D, Petit J-M, Barbaroux C, Le Thiec D, Bréchet C, Brignolas F. 2006. Impact of drought on productivity and water use efficiency in 29 genotypes of *Populus deltoides* × *Populus nigra*. *New Phytologist* **169**: 765–777.

Mulero G, Jiang D, Bonfil DJ, Helman D. 2023. Use of thermal imaging and the photochemical reflectance index (PRI) to detect wheat response to elevated CO_2 and drought. *Plant, Cell & Environment* **46**: 76–92.

Ohsumi A, Kanemura T, Homma K, Horie T, Shiraiwa T. 2007. Genotypic variation of stomatal conductance in relation to stomatal density and length in rice (*Oryza sativa* L.). *Plant Production Science* **10**: 322–328.

Pearce DW, Millard S, Bray DF, Rood SB. 2006. Stomatal characteristics of riparian poplar species in a semi-arid environment. *Tree Physiology* **26**: 211–218.

Porth I, El-Kassaby YA. 2015. Using *Populus* as a lignocellulosic feedstock for bioethanol. *Biotechnology Journal* **10**: 510–524.

Regier N, Streb S, Cocozza C, Schaub M, Cherubini P, Zeeman SC, Frey B. 2009. Drought tolerance of two black poplar (*Populus nigra* L.) clones:

contribution of carbohydrates and oxidative stress defence. *Plant, Cell & Environment* **32**: 1724–1736.

Sannigrahi P, Ragauskas AJ, Tuskan GA. 2010. Poplar as a feedstock for biofuels: a review of compositional characteristics. *Biofuels, Bioproducts & Biorefining* **4**: 209–226.

Savolainen O, Lascoux M, Merilä J. 2013. Ecological genomics of local adaptation. *Nature Reviews. Genetics* **14**: 807–820.

Schmidt T, Fernando AL, Monti A, Rettenmaier N. 2015. Life cycle assessment of bioenergy and bio-based products from perennial grasses cultivated on marginal land in the mediterranean region. *Bioenergy Research* **8**: 1548–1561.

Shepherd T, Wynne Griffiths D. 2006. The effects of stress on plant cuticular waxes: tansley review. *New Phytologist* **171**: 469–499.

Simões R, Rodrigues A, Ferreira-Dias S, Miranda I, Pereira H. 2020. Chemical composition of cuticular waxes and pigments and morphology of leaves of Quercus suber trees of different provenance. *Plants* **9**: 1165.

Somerville C, Youngs H, Taylor C, Davis SC, Long SP. 2010. Feedstocks for lignocellulosic biofuels. *Science* **329**: 790–792.

Stapley J, Reger J, Feulner PGD, Smadja C, Galindo J, Ekblom R, Bennison C, Ball AD, Beckerman AP, Slate J. 2010. Adaptation genomics: the next generation. *Trends in Ecology & Evolution* **25**: 705–712.

Street NR, Skogström O, Sjödin A, Tucker J, Rodríguez-Acosta M, Nilsson P, Jansson S, Taylor G. 2006. The genetics and genomics of the drought response in *Populus*. *The Plant Journal* **48**: 321–341.

Sun Z, Jin X, Albert R, Assmann SM. 2014. Multi-level modeling of light-induced stomatal opening offers new insights into its regulation by drought. *PLoS Computational Biology* **10**: e1003930.

Tang J, Yang X, Xiao C, Li J, Chen Y, Li R, Li S, Lü S, Hu H. 2020. GDSL lipase occluded stomatal pore 1 is required for wax biosynthesis and stomatal cuticular ledge formation. *New Phytologist* **228**: 1880–1896.

Tardieu F. 2022. Different avenues for progress apply to drought tolerance, water use efficiency and yield in dry areas. *Current Opinion in Biotechnology* **73**: 128–134.

Taylor G, Bailey-Bale JH, Klein MC, Milner S, Chen J-G, Muchero W, Freer-Smith P, Tschaplinski TJ, Tuskan J. 2024. Harnessing the power of poplar tree natural genetic variation for the development of future sustainable biofuels and bioproducts: a droughted marginal-land experiment for multi-disciplinary investigations. *bioRxiv*. doi: 10.1101/2024.01.11.575272.

Taylor G, Donnison IS, Murphy-Bokern D, Morgante M, Bogeat-Triboulot M-B, Bhalerao R, Hertzberg M, Polle A, Harfouche A, Alasia F *et al.* 2019. Sustainable bioenergy for climate mitigation: developing drought-tolerant trees and grasses. *Annals of Botany* **124**: 513–520.

Tricker PJ, Calfapietra C, Kuzminsky E, Puleggi R, Ferris R, Nathoo M, Pleasants LJ, Alston V, De Angelis P, Taylor G. 2004. Long-term acclimation of leaf production, development, longevity and quality following 3 yr exposure to free-air CO_2 enrichment during canopy closure in *Populus*. *New Phytologist* **162**: 413–426.

Tschaplinski TJ, Tuskan GA, Gunderson CA. 1994. Water-stress tolerance of black and eastern cottonwood clones and four hybrid progeny. I. Growth, water relations, and gas exchange. *Canadian Journal of Forest Research* **24**: 364–371.

Tschaplinski TJ, Tuskan GA, Sewell MM, Gebre GM, Todd DE, Pendley CD. 2006. Phenotypic variation and quantitative trait locus identification for osmotic potential in an interspecific hybrid inbred F2 poplar pedigree grown in contrasting environments. *Tree Physiology* **26**: 595–604.

Tuskan GA, Difazio S, Jansson S, Bohlmann J, Grigoriev I, Hellsten U, Putnam N, Ralph S, Rombauts S, Salamov A *et al.* 2006. The genome of black cottonwood, *Populus trichocarpa* (Torr. & Gray). *Science* **313**: 1596–1604.

U.S. Department of Energy. 2022. *Sustainable aviation fuel grand challenge roadmap: flight plan for sustainable aviation fuel report*. Washigton, DC, USA: U.S. Department of Energy.

U.S. Department of Energy. 2024. *2023 Billion-Ton Report: An Assessment of U.S. Renewable Carbon Resources*. Washigton, DC, USA: U.S. Department of Energy.

U.S. Department of Energy, U.S. Department of Transport, U.S. Department of Agriculture, U.S. Environmental Protection Agency. 2022. SAF grand challenge roadmap: flight plan for sustainbale aviation fuel. [WWW document] URL https://www.energy.gov/eere/bioenergy/articles/sustainable-aviation-fuel-grand-challenge-roadmap-flight-plan-sustainable.

Viger M, Rodriguez-Acosta M, Rae AM, Morison JIL, Taylor G. 2013. Toward improved drought tolerance in bioenergy crops: QTL for carbon isotope composition and stomatal conductance in *Populus*. *Food and Energy Security* **2**: 220–236.

Viger M, Smith HK, Cohen D, Dewoody J, Trewin H, Steenackers M, Bastien C, Taylor G. 2016. Adaptive mechanisms and genomic plasticity for drought tolerance identified in European black poplar (*Populus nigra* L.). *Tree Physiology* **36**: 909–928.

Webber MS, Watson J, Zhu J, Jang JH, Çağlayan M, Heyne JS, Beckham GT, Román-Leshkov Y. 2024. Lignin deoxygenation for the production of sustainable aviation fuel blendstocks. *Nature Materials* **23**: 1622–1638.

Wong CYS, Bambach NE, Alsina MM, McElrone AJ, Jones T, Buckley TN, Kustas WP, Magney TS. 2022. Detecting short-term stress and recovery events in a vineyard using tower-based remote sensing of photochemical reflectance index (PRI). *Irrigation Science* **40**: 683–696.

Wright IJ, Dong N, Maire V, Prentice IC, Westoby M, Díaz S, Gallagher RV, Jacobs BF, Kooyman R, Law EA *et al.* 2017. Global climatic drivers of leaf size. *Science* **357**: 917–921.

Wright IJ, Reich PB, Westoby M, Ackerly DD, Baruch Z, Bongers F, Cavender-Bares J, Chapin T, Cornelissen JHC, Diemer M *et al.* 2004. The worldwide leaf economics spectrum. *Nature* **428**: 821–827.

Wu J, Albert LP, Lopes AP, Restrepo-Coupe N, Hayek M, Wiedemann KT, Guan K, Stark SC, Christoffersen B, Prohaska N *et al.* 2016. Leaf development and demography explain photosynthetic seasonality in Amazon evergreen forests. *Science* **351**: 972–976.

Xu B, Liu D, Xu G, Zhang X, Bi L. 2013. A measurement method for contact angle based on hough transformation. *Measurement* **46**: 1109–1114.

Zhang J, Yang Y, Zheng K, Xie M, Feng K, Jawdy SS, Gunter LE, Ranjan P, Singan VR, Engle N *et al.* 2018. Genome-wide association studies and expression-based quantitative trait loci analyses reveal roles of HCT2 in caffeoylquinic acid biosynthesis and its regulation by defense-responsive transcription factors in *Populus*. *New Phytologist* **220**: 502–516.

Zhang M, Suren H, Holliday JA. 2019. Phenotypic and genomic local adaptation across latitude and altitude in *Populus trichocarpa*. *Genome Biology and Evolution* **11**: 2256–2272.

Zhou X, Jacobs TB, Xue L-J, Harding SA, Tsai C-J. 2015. Exploiting SNPs for biallelic CRISPR mutations in the outcrossing woody perennial *Populus* reveals 4-coumarate: CoA ligase specificity and redundancy. *New Phytologist* **208**: 298–301.

Zhou X, Stephens M. 2012. Genome-wide efficient mixed-model analysis for association studies. *Nature Genetics* **44**: 821–824.

Supporting Information

Additional Supporting Information may be found online in the Supporting Information section at the end of the article.

Fig. S1 Soil water potential, Davis, CA climate data and experimental design.

Fig. S2 Variance components analysis (a) and principal component analysis (PCA) (b) by trait in *Populus trichocarpa*.

Fig. S3 Comparative analysis (correlations) of traits measured in this *Populus trichocarpa* study.

Fig. S4 Genetic control of traits in the genome-wide association study of the *Populus trichocarpa* population.

Fig. S5 Quantile-quantile (QQ) plots displaying the observed vs expected $-\log_{10}$ (*P*-values) for all traits included in the genome-wide association study (GWAS).

Fig. S6 Genome-wide association study (GWAS) results for all traits measured in the *Populus trichocarpa* population.

Fig. S7 Genome-wide association study (GWAS) results for untransformed stomatal size in *Populus trichocarpa*.

Fig. S8 Observed geographical distribution of example allele in chromosome 10 (10 356 950–10 746 695) associated with stomata size and density in *Populus trichocarpa*.

Table S1 Phenotypes measured and used for analysis, including definitions, units, and time points.

Table S2 Raw phenotypes of the *Populus trichocarpa* study.

Table S3 Min/max/average for each phenotype measured in *Populus trichocarpa*.

Table S4 Drought recovery index data.

Table S5 *Populus trichocarpa* genotype information (location of origin and climate data from BioClim).

Table S6 Genome-wide association study GWAS summary of all traits measured.

Table S7 Potential candidate genes (orthologs to *Arabidopsis thaliana*), also highlighted with four categories (water, stomata, guard cells, ABA).

Table S8 NCBI SRA accession numbers and genotype IDs for RNA-Seq data in *Populus trichocarpa*.

Table S9 Differential gene expression (DEG) results for genotype with big stomata vs small stomata allele in *Populus trichocarpa*.

Please note: Wiley is not responsible for the content or functionality of any Supporting Information supplied by the authors. Any queries (other than missing material) should be directed to the *New Phytologist* Central Office.